NUMERICAL SOLUTIONS FOR DETERMINING WAVE-INDUCED PRESSURE DISTRIBUTIONS AROUND BURIED PIPELINES

by

N. W. Lai, R. F. Dominguez
and
W. A. Dunlap

Coastal and Ocean Engineering Division
Civil Engineering Department
Texas A&M University

December 1974

TAMU-SG-75-205

Partially supported through Institutional Grant 04-3-158-18
to Texas A&M University
by the National Oceanic and Atmospheric
Administration's Office of Sea Grants
Department of Commerce

$3.00

Order from:

Department of Marine Resources Information
Center for Marine Resources
Texas A&M University
College Station, Texas 77843

ABSTRACT

Numerical models using both the finite difference and finite element technique are developed to simulate the interaction of a two-dimensional pipe-soil-wave system. The wave-induced pressure distribution in the soil region without an embedded pipe is first studied and solutions validated by comparing with existing analytical and experimental results. Numerical models are then used to solve the dynamic pressure distribution around buried pipes.

Results are obtained for both a square pipe and a circular pipe and comparisons are made for different cases of input wave and soil parameters. It is found that the embedded pipe causes an increase of pressure at the top region of the pipe and a decrease at the bottom. Pressure changes predicted by the finite difference approach are slightly different from the finite element results. Parameter studies are conducted to determine the influence of some of the significant factors on the pressure distribution pattern around the buried pipe.

PREFACE

This is the second in a series of reports describing the results of a research study conducted by personnel of the Civil Engineering Department at Texas A&M University on Offshore Pipelines. The study is funded by institutional grant 04-158-18 to Texas A&M University by the National Oceanic and Atmospheric Administration's Office of Sea Grants, Department of Commerce. The task of this project is to develop improved design procedures for offshore pipelines. The first report of this project, entitled "A Bibliography of Offshore Pipeline Literature", contained approximately 400 pertinent references on offshore pipelines arranged under the headings of various key topics. A third report is in preparation covering the experimental phase of the study, which involved measurement of fluid pressures in a pervious medium subjected to wave action. The study was conducted in a laboratory flume.

The authors would like to thank Professor Robert O. Reid, Department of Oceanography, for his effort and time spent in reviewing this report. The helpful suggestions and comments of Dr. Charles F. Kettleborough, Department of Mechanical Engineering, are also sincerely appreciated.

TABLE OF CONTENTS

TABLE OF CONTENTS (CONTINUED)

LIST OF TABLES

LIST OF FIGURES

LIST OF FIGURES (CONTINUED)

LIST OF FIGURES (CONTINUED)

CHAPTER I

INTRODUCTION

Although major advancements in offshore pipelining technology have been made in the last decade, severe storms still pose a significant hazard as witnessed by recent recorded failures (3). Pipelines, which are usually laid on the sea bottom, are exposed to the destructive forces of waves and currents. Huge waves produced by hurricanes induce significant bottom fluid velocities often causing severe damage to unburied pipelines even in great depths. Movements of pipelines were recorded in 240 feet of water during the passage of Hurricane Betsy (3). The ASCE Task Committee on Flotation Studies (1) reported that unburied pipeline sections were moved as far as 1400 feet under the influence of Hurricane Flossy in 1956. The more than $200 million loss in pipeline facilities sustained off the Gulf Coast during 1964 and 1965 from two major hurricanes attests to the importance of environmental factors in offshore pipeline operations. In order to protect pipelines from these hostile forces of nature, offshore operators in recent years have indicated a growing recognition of the need for burying submerged lines.

Pipeline burial is a complicated problem to deal with. It involves a three-way interaction among the buried pipe; the soil

---

The citations on the following pages follow the style of the Journal of the Hydraulics Division, Proceedings of the American Society of Civil Engineers.

sediments around it; and the hydrodynamic forces produced by surface waves. Pipelines that are adequately buried normally have minimal hydrodynamic forces exerted upon them. However, the action of erosion and liquefaction caused by wave agitation can still be quite effective down to a significant depth in the soil on certain occasions. So far, pipeliners have been unable to define a complete mechanistic picture of what actually happens when a buried pipeline fails. Their engineering design on this phase of pipeline stability has been based largely on empirical results and experience. It is of vital importance to the pipeline industry to maintain continuous operations and structural integrity of their pipelines. As pipeline burial is an expensive operation, pipeline failures often result in very costly repairs and production losses. There now exists an urgent need to develop a rational design procedure to predict the required stability conditions for burying pipelines.

Several analytical methods have been proposed for determining the velocity and pressure distributions in and near a porous sea bed. As yet, no one result has been conclusive. The study of wave-induced porous flow depends upon the assumed laws of hydrodynamics in the permeable medium and the boundary conditions at the interface. The addition of a foreign body - the buried pipeline - tends to make the problem more complex. It is the objective of this study to investigate wave-induced dynamic pressure distributions in the soil media in the immediate vicinity of the pipelines. Numerical models using both the finite difference and finite element technique are developed

to simulate the pipe-soil-wave system. The dynamic damping of wave pressure through soil sediment and its distribution around an embedded impervious object - the pipeline - are obtained. By varying the wave, soil and pipe conditions, parametric relations which may help to explain pipeline dynamics can be determined. Comparisons with experimental results are made possible by a wave-tank laboratory study conducted at the same time. By knowing the flow patterns and pressure distributions around the pipeline, failure mechanisms of scouring and liquefaction can then be explored through continued research. This study is considered as an initial step in pipeline stability research, and is intended to help provide insight into the complicated pipeline burial problem.

CHAPTER II

LITERATURE SURVEY

Wave Damping Studies

Most of the classical theories dealing with the movement of waves in shallow water assume that energy is neither gained nor lost during their travel, and that the vertical component of fluid particle velocity is zero at the bottom. But recent studies have shown that the oscillatory motion of waves and the associated translating pressure differentials along a porous sea bed can induce percolation of bottom water in and out of the bed. A significant loss of wave energy can occur due to a dissipating mechanism actuated by the induced porous flow. The damping of waves approaching the shore and the erosion of bottom sediments are only two of the problems which may be affected by bottom percolation.

The effect on the surface wave as a result of viscous damping induced in a permeable bed was first studied by Putman (15) in 1949. In his study, he assumed a horizontal sea bottom with permeable material (sand) having uniform permeability. By applying Darcy's Law for the fluid flow through the porous medium and analyzing the problem as one of potential flow, he derived an equation for the wave energy dissipation function. He went on to show that this loss of wave energy can be reflected in the reduction of wave height due to the dissipation of mechanical energy accompanying the viscous

flow of fluid within the sand medium.

In 1957, Reid and Kajiura (16) re-examined Putnam's approximate method by using a more rigorous approach. They found that his analysis was justified in view of the smallness of the permeability factors commonly encountered. They also showed that Darcy's Law is an adequate approximation for unsteady porous flow for this problem. However, in both papers, they used only the classical irrotational and inviscid wave solution above a region of viscous porous flow, with continuity in pressure and vertical velocity assumed at the fluid-soil interface. This leads to a solution in which there is a discontinuity in the horizontal component of velocity at the interface.

Later , Hunt (10) added in the effect of viscosity on the damping characteristics of such waves, and stated that this would reduce the horizontal velocity to zero at the interface. But his solution still showed a discontinuity of the horizontal velocity at the interface, and his velocity components in the upper water are not affected by the permeable bed, which is most unlikely.

Murray (14) in 1965 studied the same problem but used a different set of boundary conditions at the bed surface. He suggested matching the velocity components in the permeable material at the interface. Conservation arguments and consideration of the rate of doing work at the fluid-bed interface were applied in his analysis. His solution of the damping characteristics are different from that given in previous studies. He also showed that stresses are not

continuous at the interface as was assumed by Hunt. It is to be noted, however, that the equations of motion in the permeable bed used in Murray's paper are somewhat confusing. Instead of using the specific velocity in the linearized friction terms, he used the seepage velocity, and therefore, the limiting case when the frequency becomes infintely small cannot be reduced to the well-known Darcy's Equation.

In 1973, Liu (13) used the equations of motion for the permeable medium as appeared in Reid and Kajiura's paper, and he solved the porous flow problem by employing a Boundary-Layer-Approximation approach. Continuity of pressure and velocity components are required as boundary conditions at the interface only up to the order of $\sqrt{\nu}$. He arrived at approximate solutions for the velocity field in the porous medium, dependent on the porosity of the bed material.

An experimental attempt to verify the damping rate predicted by Putnam was made by Savage (17) in 1953. His results were in marked disagreement with Putman's formula, but may have been affected by uncertainties in the elimination of the effect of friction, the observed instability of the wave train, and the fact that the coefficient of permeability of the bed was not determined in situ.

Sleath (20) in 1970 carefully measured the pressure distribution in the bed directly in a model study by installing pressure transducers on the side wall of a wave channel. He showed that stratification of sand in the model bed would cause the mean permeability in the horizontal direction to be different from that in

the vertical direction, which is usually assumed to be uniform in all the other studies. Comparisons of experimental results with theory based on Putnam's work which accounted for this difference showed good agreement.

Soil Stability Studies

Unstable bottom soil conditions have often caused severe damage to offshore pipelines even though they were buried. Sections of pipelines can be moved or floated to the surface by mysterious forces during storm conditions. Recently, researchers have developed interest in one unique type of soil failure --- sliding or mass movement of sea-bed sediments. This sliding phenomenon is initiated by waves of sufficient height and period to produce significant pressures on the sea floor. If the surface waves exert enough pressure, the soil may become unstable. The magnitude of soil movement induced may provide large enough lateral forces to cause pipeline failures. Bea (2) described in his paper how these land slides damaged two offshore production platforms. Henkel (9) developed an analytical procedure to predict the conditions under which wave-induced slides might be expected.

Scouring is another phenomenon affecting buried pipeline design considerations. Scouring involves the large scale transport of the sea-bed sediments due to a momentum exchange between rapidly moving water and the individual grains that form the bed. Sea floor scouring is most prevalent during storm conditions which generate

high bottom velocities required to remove the backfilled materials of pipelines. Once exposed, the pipe becomes subjected to the direct action of current forces which can cause the pipe to move.

Another form of possible failure is pipeline flotation. Flotation is often caused by a phenomenon known as soil liquefaction. This phenomenon occurs when the pore fluid pressures in the soil induced by repeated cyclic wave loadings become equal to the total overburden stresses, reducing the effective shear stresses in the soil to zero. During liquefaction, the soil sediments behave very much like a dense fluid, and the resulting suspension may have a unit weight high enough to immediately float the pipeline. There is a critical density of the soil and water mixture at which the buried pipeline will begin to float through its cover. Brown (6) has presented a standard type of soil test to determine specific gravities required, inferring methods of backfilling and depth of burial. The ASCE Pipeline Flotation Research Committee (1) has published "state-of-the-art" tables that yield the necessary specific gravity for a pipe to stay buried and to keep it from sinking in agitated sediments. Research on soil liquefaction has been done by Seed (18) and many others, but a complete mechanistic picture of its interaction with buried pipelines is still lacking, making it necessary to rely on pipeline weighting or the use of anchors to hold the pipeline in place.

CHAPTER III

DEVELOPMENT AND DESCRIPTION OF THE NUMERICAL MODEL

Problem Statement

It is the purpose of this study to develop a numerical model for determining wave-induced pressure distributions around a buried pipeline. Consider Fig. 3.1, which shows a two-dimensional sinusoidal wave in a fluid layer of mean depth h, overlying a homogeneous porous medium of infinite depth. A pipe of diameter D is embedded in the porous medium at a burial depth d. The surrounding fluid has a kinematic viscosity ν, and the porous medium a permeability K and porosity n which describe the fluid flow rate and void volume of the medium respectively. The x-axis lies at the mean free water surface, and the y-axis is taken to be directed vertically upwards. We shall be concerned with small amplitude, progressive plane waves advancing in the direction of the x-axis.

The problem involves interaction between the buried pipe and its surrounding porous material with the surface wave acting as hydrodynamic loading on the system. Velocity and pressure distribution in the upper fluid layer are influenced by percolations in the lower porous layer, and those in this lower layer are in turn influenced by the buried pipe. As waves pass over the porous bed, pressure fluctuation on the fluid-bed interface induce a viscous flow within the porous medium, causing dissipation of mechanical energy

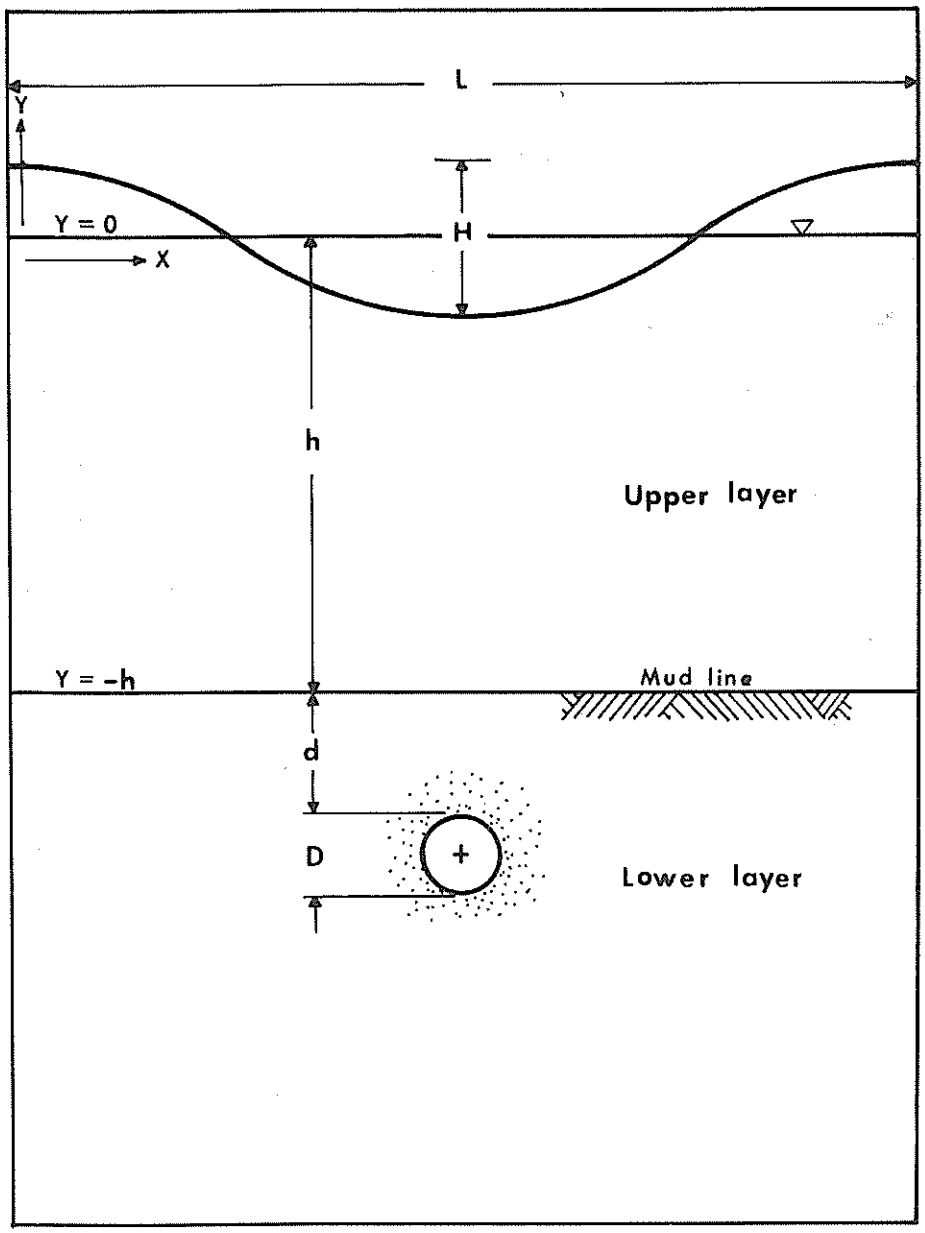

Fig. 3.1 - Definition Sketch

and thus damping of the waves. The orbital motion of the fluid particles is quickly damped as they travel from the upper fluid layer into the porous medium as shown in Fig. 3.2. Liu's equation for pressure distribution in the porous medium is plotted in Fig. 3.3, showing the exponential damping of dynamic wave pressure with depth at a specific instant of time. It can be expected that the pressure field will be altered to some degree if an impervious object such as a pipe is placed in the upper region of the bed. An understanding of the pressure distribution pattern around the pipe is important for determining the wave forces acting on the pipe as well as the effective stresses that exist in the bed.

A region containing the homogeneous bed and embedded pipe will be considered in the development of a two-dimensional numerical model for this study as in Fig. 3.5 (p.16). From here on, this region will be referred to as the problem region in this report. Suitable boundary conditions will be imposed for each individual situation encountered. The problem is actually treated in a steady state sense as solutions give pressure distributions for a specified instant of time. A dynamic time dependent situation can be simulated by changing the pressure wave profile which is imposed as an upper boundary condition in the problem (Fig. 3.4). However, complete pressure dissipation is assumed in each case, which precludes the build-up of pore water pressure in the bed materials.

Governing Equations

In most practical situations the Reynolds number is based on

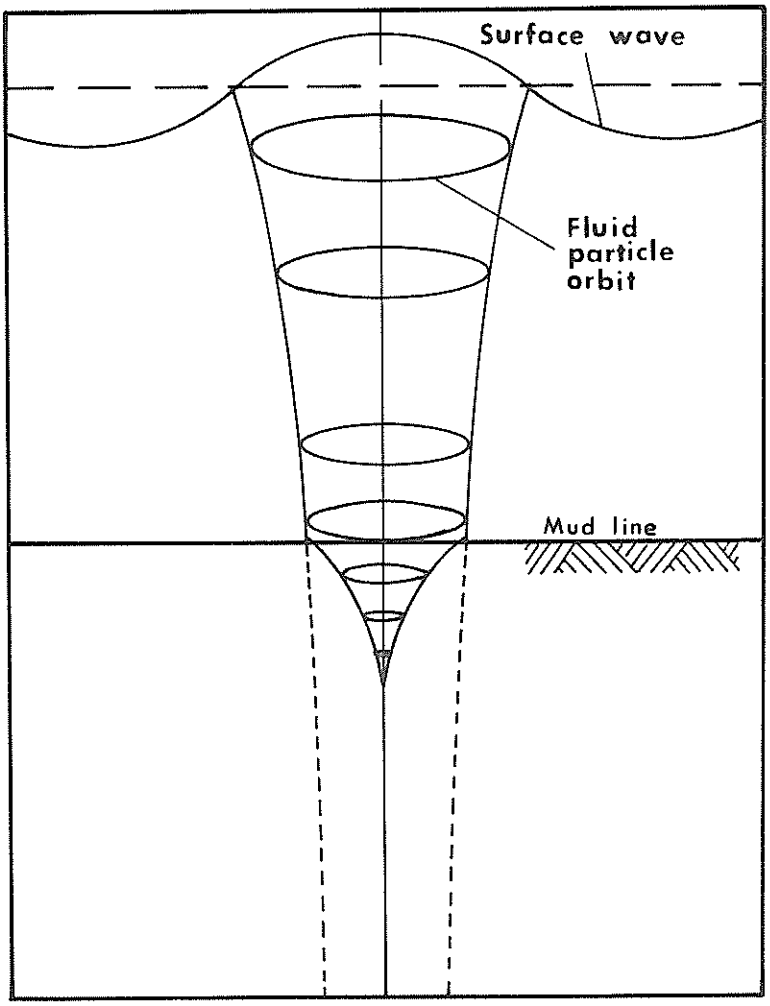

Fig. 3.2 - Schematic Representation of Fluid Particle Orbits in the Fluid and Soil Media

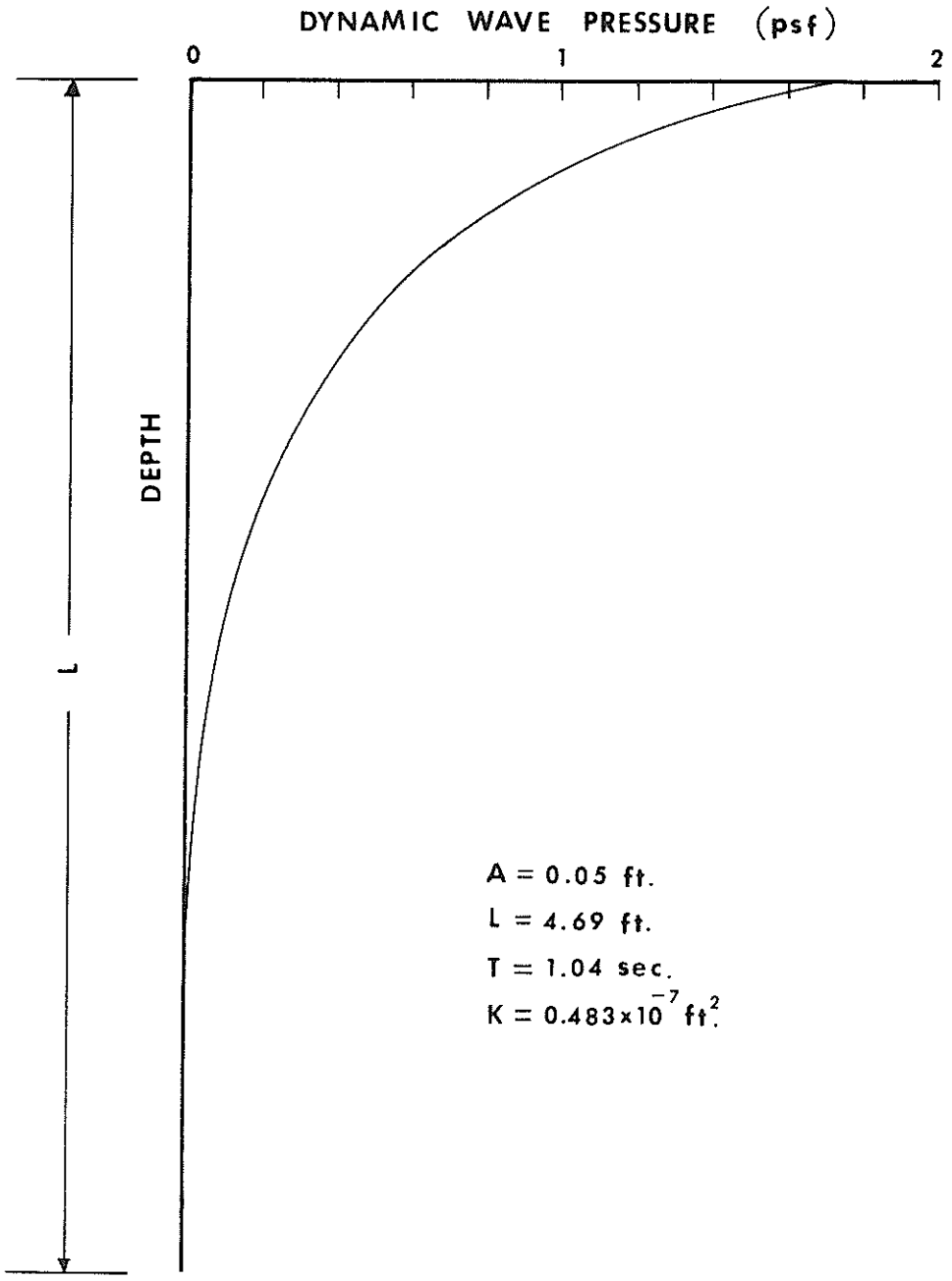

Fig. 3.3 - Damping of Wave Pressure through Soil by Liu's Analytical Solution

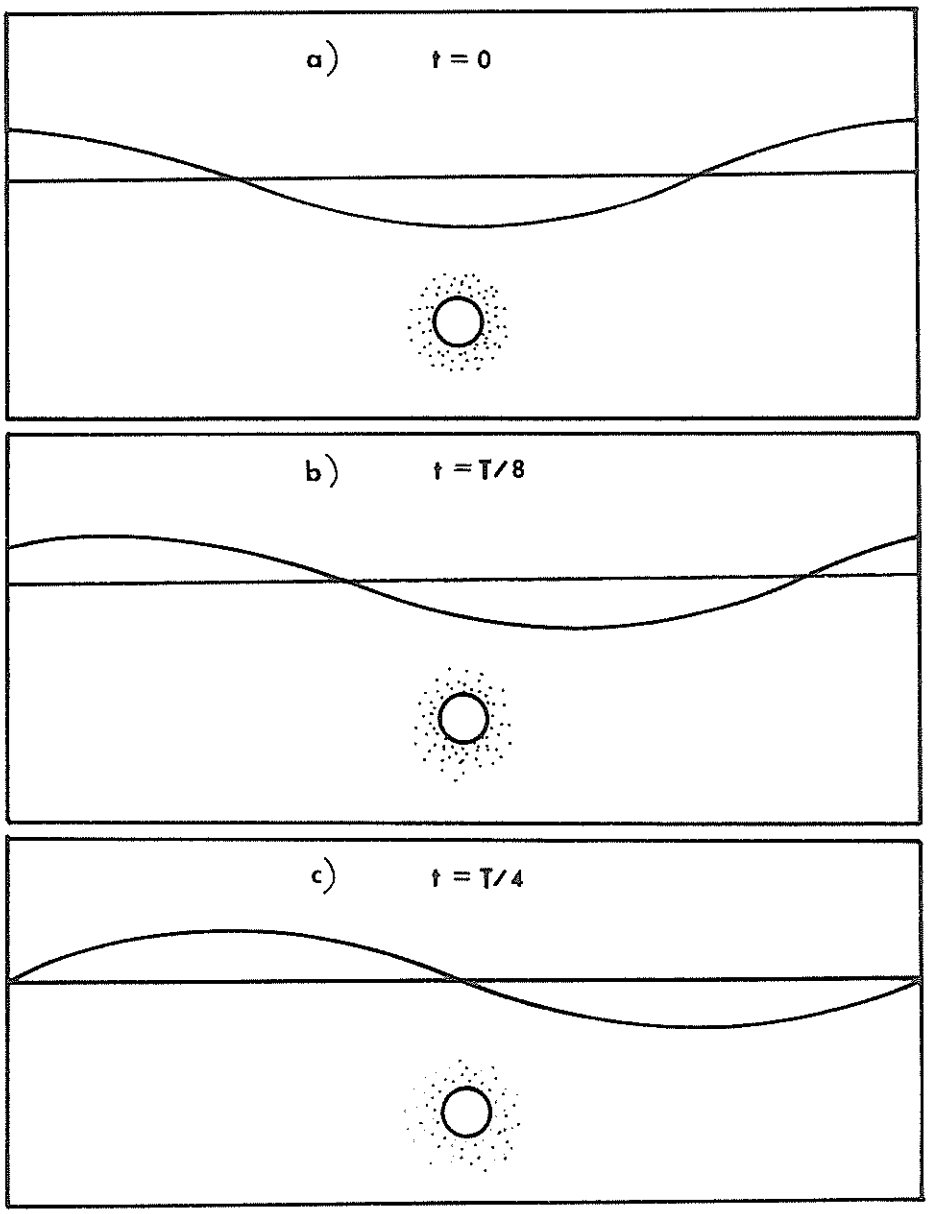

Fig. 3.4 - Change of Wave Profile Position with Time

grain size and superficial velocity. For viscous flow in a porous bed, the Reynolds number will be less than unity and Darcy's Law becomes applicable. The following is the form of Darcy's equation utilized by Reid and Kajiura (16):

$$\frac{1}{n}\frac{\partial u}{\partial t} = -\frac{\nu}{K}u - \frac{1}{\rho}\frac{\partial p}{\partial x} \quad \ldots\ldots\ldots\ldots\ldots (3.1)$$

$$\frac{1}{n}\frac{\partial v}{\partial t} = -\frac{\nu}{K}v - \frac{1}{\rho}\frac{\partial p}{\partial y} \quad \ldots\ldots\ldots\ldots\ldots (3.2)$$

where u and v are velocity components in the x and y directions, p is the dynamic pressure which is the object of concern, and ν and ρ are the kinematic viscosity and density respectively of the fluid. It is assumed that the porous medium is homogeneous, so that the permeability K and porosity n are constant and non-directional. For unaccelerated flows Eqs. 3.1 and 3.2 can be reduced to the more common form of Darcy's equation:

$$u = -\frac{K}{\nu\rho}\frac{\partial p}{\partial x} \quad \ldots\ldots\ldots\ldots\ldots (3.3)$$

$$v = -\frac{K}{\nu\rho}\frac{\partial p}{\partial y} \quad \ldots\ldots\ldots\ldots\ldots (3.4)$$

If the fluid is considered incompressible, the flow in the porous medium must satisfy the Continuity equation of the form

$$\frac{\partial u}{\partial x} + \frac{\partial v}{\partial y} = 0 \quad \ldots\ldots\ldots\ldots\ldots (3.5)$$

Differentiating Eqs. 3.1 and 3.2 and substituting into Eq. 3.5 gives

the Laplace equation

$$\frac{\partial^2 p}{\partial x^2} + \frac{\partial^2 p}{\partial y^2} = 0 \quad \ldots\ldots\ldots\ldots\ldots\ldots \quad (3.6)$$

or $$\nabla^2 p = 0 \quad \ldots\ldots\ldots\ldots\ldots\ldots \quad (3.7)$$

which governs the distribution of pressure p in the porous medium.

Boundary Conditions

In order to solve the Laplace Equation (Eq. 3.6), a zone defining the problem region shown in Fig. 3.5 is considered.

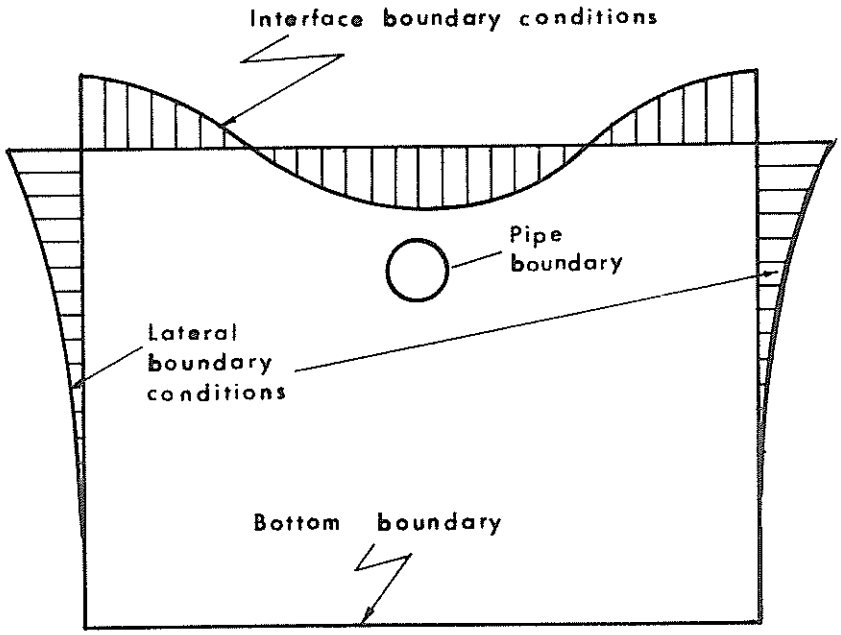

Fig. 3.5 - Problem Region Boundary Conditions

Interface Boundary Conditions

The top boundary of the problem region represents the fluid-bed interface of the model. Its width is taken to be one wavelength L long. The pressure variation at that surface must be defined and imposed as a boundary condition for both the finite difference and finite element numerical models which are used in this study.

Several theories were considered which may be utilized to give pressure variations at this interface boundary. An equation can be developed from the Linear Wave Theory (11) for the dynamic wave pressure p_1 in the upper fluid layer as

$$p_1 = \rho g \left[A \cos (kx - \sigma t) \frac{\cosh k (y+h)}{\cosh kh} \right] . \quad . \quad . \quad . \quad (3.8)$$

where g is the acceleration of gravity, A the wave amplitude, k the wave number and σ is the radian wave frequency. The subscript 1 is used to indicate the upper fluid layer (see Fig. 3.1) and 2 refer to the lower porous medium. If y = -h, then p_o will be the pressure variation along the interface describable as

$$p_o = \rho g \left[\frac{A \cos (kx - \sigma t)}{\cosh kh} \right] . \quad . \quad . \quad . \quad . \quad . \quad . \quad . \quad . \quad . \quad (3.9)$$

Since Linear Wave Theory assumes an impervious bottom condition, it becomes inadequate in describing the problem under consideration.

Sleath (20) took into consideration a stratified porous bottom layer and obtained an equation for the general pressure distribution in the porous medium as follows:

$$p_2 = \frac{A\rho g}{\cosh kh}\left[\frac{\cosh k\left(\frac{K_x}{K_y}\right)^{\frac{1}{2}}(y+h+b)}{\cosh k\left(\frac{K_x}{K_y}\right)^{\frac{1}{2}} b}\right]\cos(kx-\sigma t) \quad . . \quad (3.10)$$

where b is the depth of the porous layer, K_x and K_y are the permeability coefficients in the x and y directions respectively. By setting y = -h, Eq. 3.10 can also be reduced to give the pressure variation along the interface as:

$$p_o = \frac{A\rho g}{\cosh kh}\left[\cos(kx-\sigma t)\right] . . . . . \quad (3.11)$$

His study over-simplified the problem as he assumed an invicid irrotational wave solution above a region of viscous porous flow. The permeability K term drops out of Eq. 3.10 when y is set equal to -h, reducing it to that predicted by the Linear Wave Theory (Eq. 3.9).

Liu (12) considered the viscous effect in both the upper fluid layer and the lower porous medium and developed equations for the pressure field in both regions as follows:

$$p_1 = \left(\frac{i\rho Ag}{D}\right)\left[\left(\frac{\sigma}{Q}\sinh k(y+h) - i\cosh k(y+h)\right)\exp\left[i(kx-\sigma t)\right]\right] . . . . . \quad (3.12)$$

$$p_2 = \left(\frac{pAg}{D}\right)\exp\left[k(y+h)\right]\exp\left[i(kx-\sigma t)\right] . . . . . \quad (3.13)$$

where $D = \cosh kh + \left(\frac{\sigma}{Q}\right)\sinh kh$ . . . . . (3.14)

and $$Q = -\frac{\nu}{K} \quad \ldots\ldots\ldots\ldots\ldots\ldots\ldots\ldots \quad (3.15)$$

After rearranging and retaining only the positive parts of Eqs. 3.12 and 3.13, the following is obtained.

$$p_1 = \frac{\rho A g}{D}\left[\cos\,(kx-\sigma t)\,\cosh\,k(y+h) - \frac{\sigma}{Q}\sin\,(kx-\sigma t)\sinh\,k(y+h)\right] \quad \ldots\ldots\ldots\ldots\ldots\ldots \quad (3.16)$$

$$p_2 = \frac{\rho A g}{D}\left[\cos\,(kx-\sigma t)\,\cosh\,k(y+h) + \cos\,(kx-\sigma t)\,\sinh\,k(y+h)\right] \quad \ldots\ldots\ldots\ldots\ldots\ldots \quad (3.17)$$

By setting $y = -h$, the pressure variation at the fluid-bed interface can be given by either one of the above equations as

$$p_o = \frac{\rho A g}{D}\left[\cos\,(kx-\sigma t)\,\cosh\,k(y+h)\right] \quad \ldots\ldots\ldots \quad (3.18)$$

Eq. 3.18 will be used to provide the interface boundary conditions for the problem region in the numerical study.

Lateral Boundary Conditions

Lateral boundary values of the problem region in Fig. 3.5 can also be determined from Eq. 3.17 by varying y for a given time t if fixed boundaries are desired. Since the width of the problem region is taken to be one wavelength both the left and right boundary values are identical. Another approach can thus be made by using a

successive boundary condition in which boundary values on one side are set equal to those on the other.

Pipe Boundary Conditions

The pipe will be located at the center of the problem region but can be moved vertically along the y-axis to simulate the depth of burial of the pipe. The pipe is considered to be impervious and Boundary Layer Theory applies for the region associated with the pipe surface.

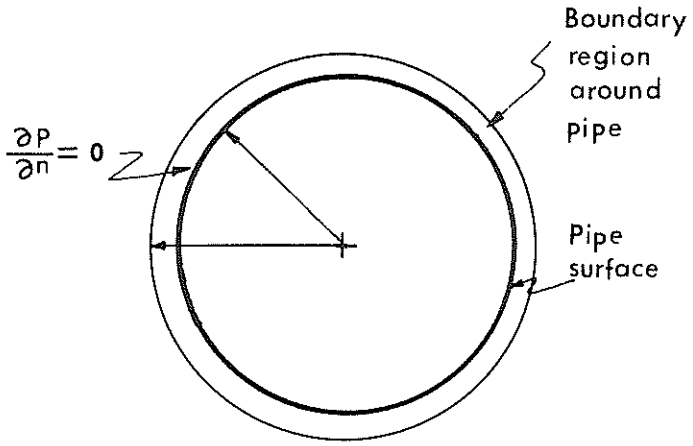

Fig. 3.6 - Pipe Boundary Conditions

According to classical theory, the pressure within the boundary layer is approximately constant in the direction normal to the surface. Hence a normal derivative boundary condition

$$\frac{\partial p}{\partial n} = 0 \quad \ldots\ldots\ldots\ldots\ldots\ldots \quad (3.19)$$

has to be satisfied on the pipe surface. Here, n will be used to denote the normal direction radially outward from the pipe surface.

Bottom Boundary Conditions

The vertical extent of the flow field in this study is flexible. Different bottom boundary conditions can be imposed on the problem region to simulate variations of bottom soil conditions. In Fig. 3.3, it can be seen that the dynamic pressure value is almost damped to zero at a depth of about one wavelength as is predicted by Eq. 3.17. In a large part of this numerical study, a depth of one wavelength is considered, thus the flow field of interest becomes a square region and zero pressure values can be used as bottom boundary conditions. However, in some cases, an impervious bottom layer may be encountered at a depth less that L. Thus the normal derivative condition for the pressure

$$\frac{\partial p}{\partial n} = 0 \quad \ldots\ldots\ldots\ldots\ldots\ldots\ldots\ldots \quad (3.20)$$

can be imposed as a boundary condition at the bottom.

CHAPTER IV

FINITE DIFFERENCE APPROXIMATION

Normalization of Governing Equations

Eq. 3.6 can be expressed in non-dimensional form by introducing suitable dimensionless variables. Dimensionless distances and pressure shall be defined as:

$$\bar{x} = \frac{w}{x} \qquad 0 \leq \bar{x} \leq 1$$
$$\bar{y} = \frac{B}{y} \qquad 0 \leq \bar{y} \leq 1 \qquad \ldots\ldots (4.1)$$
$$\bar{p} = \frac{p'}{p}$$

where p' is the hydrostatic pressure and W and B are the width and height of the problem region considered (Fig. 4.1).

With these dimensionless variables the Laplace equation (Eq. 3.6) can be written as

$$\frac{p'}{B^2}\frac{\partial^2 \bar{p}}{\partial x^2} + \frac{p'}{W^2}\frac{\partial^2 \bar{p}}{\partial \bar{y}^2} = 0 \qquad \ldots\ldots\ldots\ldots (4.2)$$

or

$$\frac{\partial^2 \bar{p}}{\partial \bar{x}^2} + \left(\frac{B}{W}\right)^2 \frac{\partial^2 \bar{p}}{\partial \bar{y}^2} = 0 \qquad \ldots\ldots\ldots\ldots (4.3)$$

For convenience, the bar notation associated with the dimensionless quantities will be dropped in the following sections with the understanding that dimensionless x,y and p are used throughout the chapter.

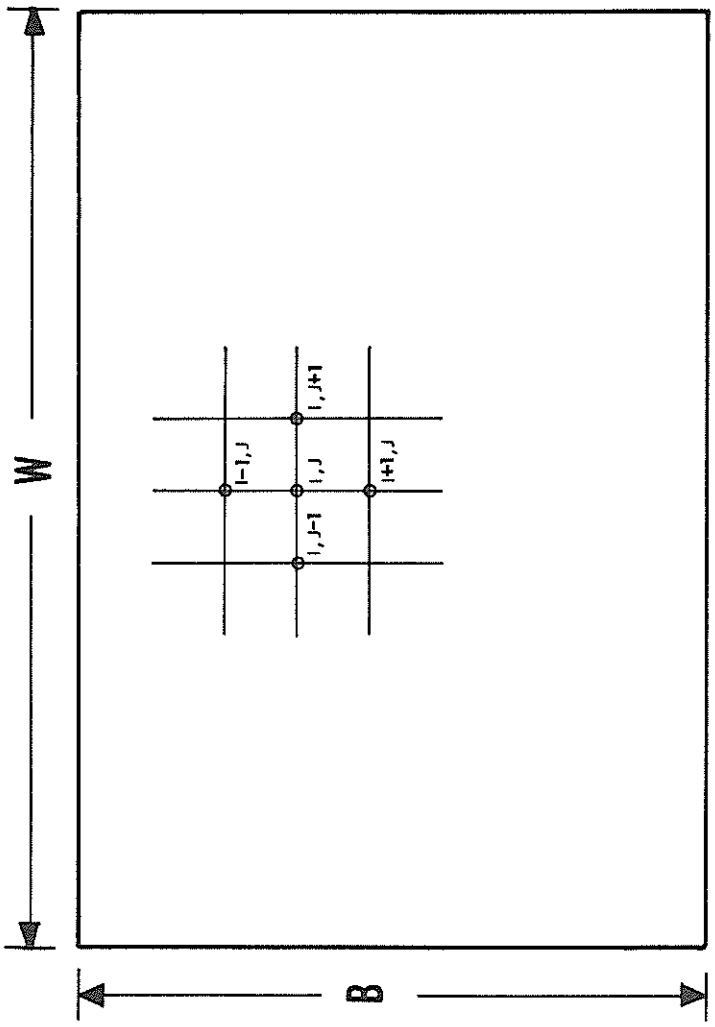

Fig. 4.1 - Dimensions of the Problem Region

Grid Point System

In the numerical solution of a partial differential equation the dependent variables are assumed to exist at a finite number of regularly spaced values of the independent variables known as grid points. The derivatives are replaced by finite difference and the differential equation is then replaced by an algebraic equation which is to be solved numerically. Before attempting to derive the finite difference approximation of the derivatives, it is necessary to define a grid point system in the region occupied by the independent variables.

The main objective of this study is to determine the pressure field near the pipe. For this reason, the grid system is designed to have a finer mesh immediately around the pipe, offering smaller spacings and thus more points of interest in that region. Fig. 4.2 and Fig. 4.3 show grid point systems around a square pipe and a circular pipe respectively. In both cases, finer meshes surrounding the pipe can be formed by subdividing the regular grid system. Subscripts (i, j) denote the grid point positions with i indicating the row and j the column of the system. Grid sizes can be determined by dividing the width and height of the problem region by the number of spacings in each direction.

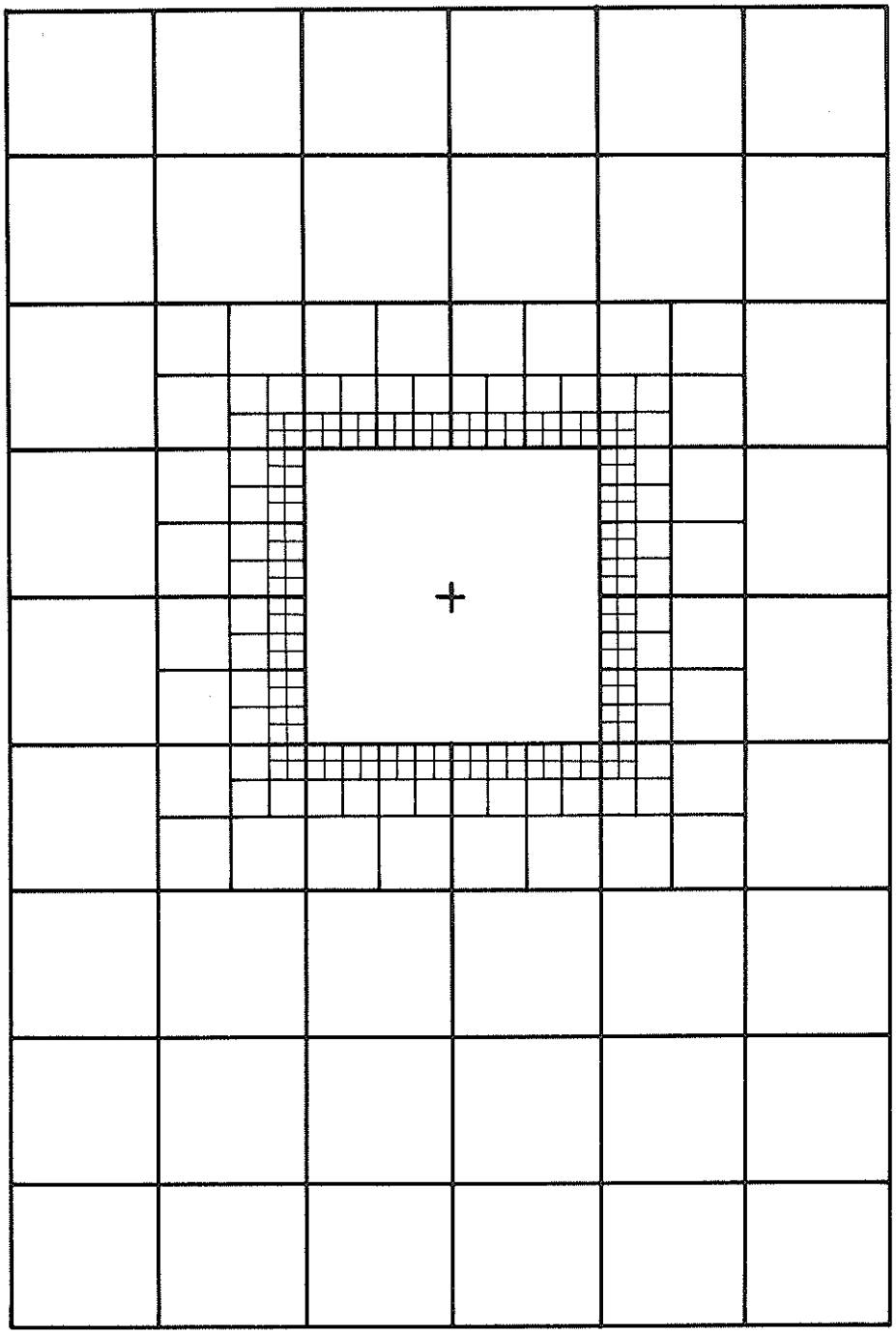

Fig. 4.2 - Grid System around a Square Pipe
(Finite Difference Method)

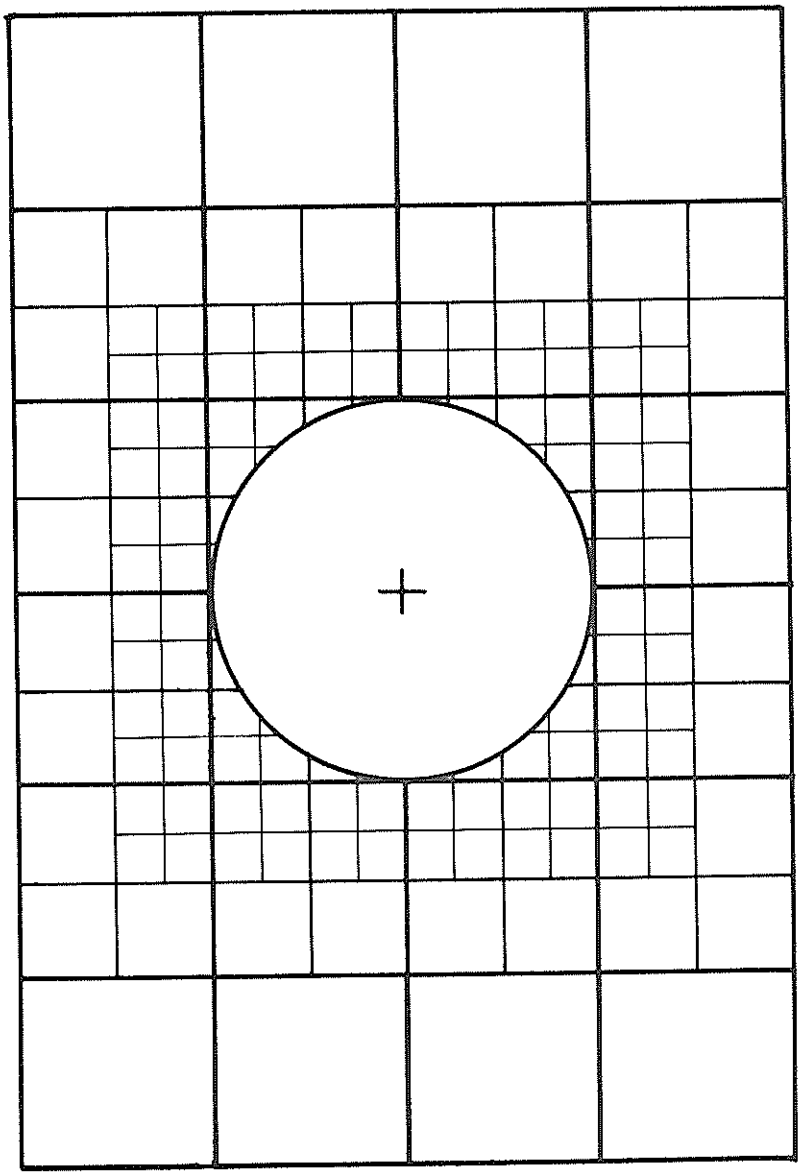

Fig. 4.3 - Grid System around a Circular Pipe
(Finite Difference Method)

Equations for Derivatives in Finite Difference Form

Finite Difference Form of the Governing Equations

The basic principle in extablishing a finite difference approximation to the derivatives of a dependent variable at a point is the application of a Taylor's series expansion to the value of that variable in the vicinity of that point.

Fig. 4.4 shows a set of grid points with spacings of Δx and Δy in the x and y directions respectively.

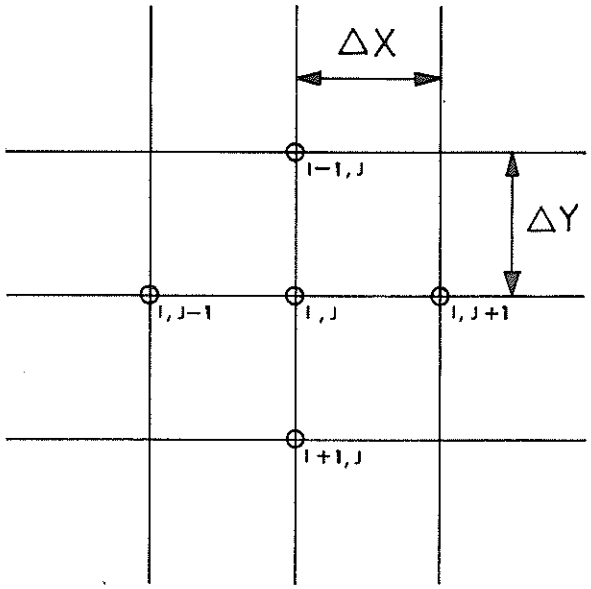

Fig. 4.4 - Arrangement of Grid Points

Eq. 4.3 can be written in finite difference form by using a

three-point central differences approximation as

$$\frac{p_{i,\,j+i} - 2p_{i,j} + p_{i,\,j-1}}{\Delta x^2} + \left(\frac{B}{W}\right)^2 \frac{p_{i-1,\,j} - 2p_{i,j} + p_{i+1,\,j}}{\Delta y^2} = 0 \quad \ldots\ldots (4.4)$$

Rearranging, we have

$$p_{i,j} = \frac{(p_{i,\,j+1} + p_{i,\,j-1}) + ER(p_{i-1,\,j} + p_{i+1,\,j})}{2(1+ER)} \quad . (4.5)$$

where $E = (B/W)^2$ and $R = (\Delta x/\Delta y)^2$ $\ldots\ldots\ldots\ldots (4.6)$

Hence the value of p at a point (i, j) can be determined if the conditions of its neighboring points are known.

Finite Difference Forms of Boundary Conditions on Pipe Surfaces

Pipes having different geometric configurations require a different formulation technique for developing the finite difference equations on the pipe boundaries. For the immediate purpose, a square pipe will first be considered as it presents a simple geometric form to to solved.

Square Pipe. Fig. 4.5 shows a scheme of boundary points that can be imposed on the surface of a square pipe. Nodal points (4, 0 and 2) are grid points lying on the pipe surface. Point 1 is a fictitious point inside the pipe. In order to develop a finite difference equation for point 0, the following procedure is taken:

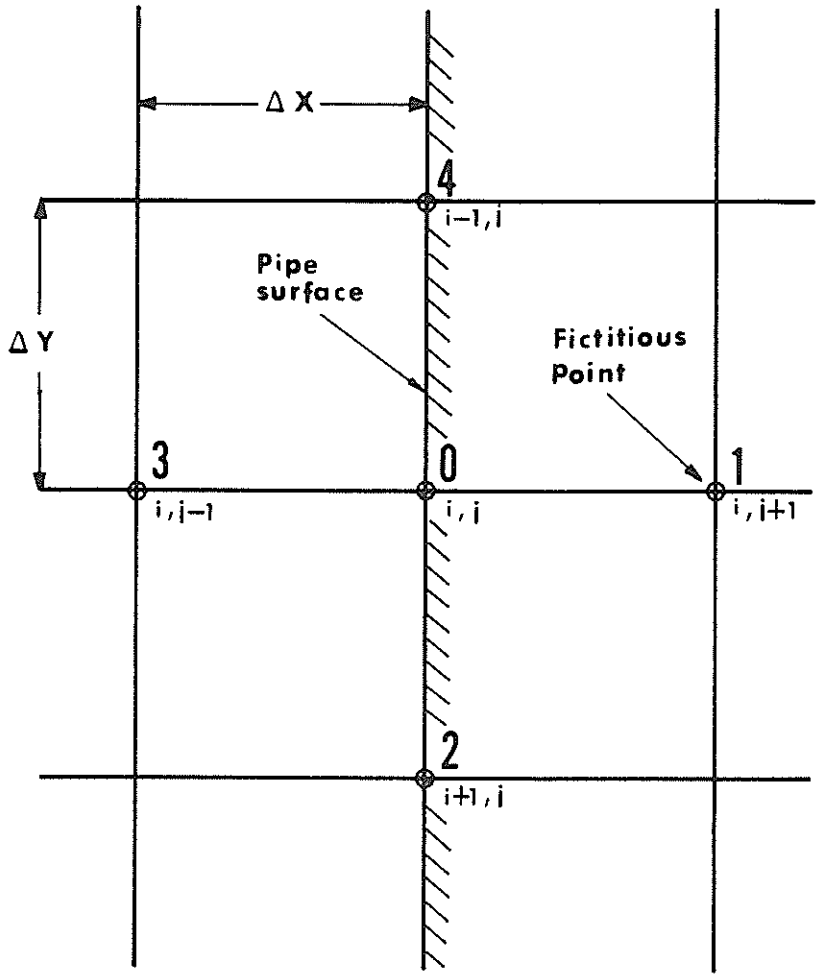

Fig. 4.5 - Boundary Grid Points on Surface of a Square Pipe

Taking the normal derivative in the x-direction, we can write Eq. 3.19 as:

$$\frac{\partial p}{\partial x} = 0 \quad \ldots\ldots\ldots\ldots\ldots\ldots \quad (4.7)$$

By using a forward difference approximation, this can be written in finite difference form

$$\frac{p_1 - p_3}{2\Delta x} = 0 \quad \ldots\ldots\ldots\ldots\ldots \quad (4.8)$$

or

$$p_1 = p_3 \quad \ldots\ldots\ldots\ldots\ldots\ldots \quad (4.9)$$

The fictitious point 1 can be eliminated and replaced by point 3. This approximation is acceptable only if the grid spacing Δx is in the order of the boundary layer thickness around the pipe.

Substituting Eq. 4.9 into Eq. 4.5 we have a finite difference equation for the boundary point 0.

$$p_{i,j} = \frac{2p_{i,j-1} + ER(p_{i-1,j} + p_{i+1,j})}{2(1 + ER)} \quad \ldots\ldots \quad (4.10)$$

Likewise, finite difference equations can be determined for all the other boundary points on the pipe surface.

Circular Pipe. Since a circular pipe boundary is considered to be irregular, it is usually difficult to arrange for the pipe surface to fall at regularly spaced grid points. Therefore, a different technique has to be developed for writing finite difference equations for boundary points on the curve surface.

Fig. 4.6 shows a scheme of grid points imposed on the circular pipe. For simplicity of presentation, let us consider square grids and assume spacings comparable to the boundary layer thickness on the pipe surface. Points 1 - 24 are grid points that are lying on or very close to the circular boundary. Points a - p are fictitious grid points inside the circular pipe. Points A - T lie on normal direction vectors joining the inner fictitious lines with outer regular grids. One difficulty introduced into this problem comes from the irregular stars at points 2, 3, 4, etc. Considering point 2 for example, the finite difference expression for that point includes the value of fictitious point p. In the last section, for the case of a square pipe, this was eliminated by using the specified normal derivative condition of pressure values at that surface. Now, however, point p does not lie on the normal direction vector connecting point 2, so that a different treatment has to be presented.

Introducing a point A as shown in Fig. 4.6, line A-2 is normal to the pipe surface. By using the Linear Interpolation Method, we have:

$$p_A = p_1 + (p_p - p_1) \frac{A1}{p1} \quad \ldots\ldots\ldots\ldots (4.11)$$

or

$$p1\ (p_A) = AP\ (p_1) + A1\ (p_p) \quad \ldots\ldots\ldots\ldots (4.12)$$

Also, to the same order of approximation, the normal derivative boundary condition can be written as:

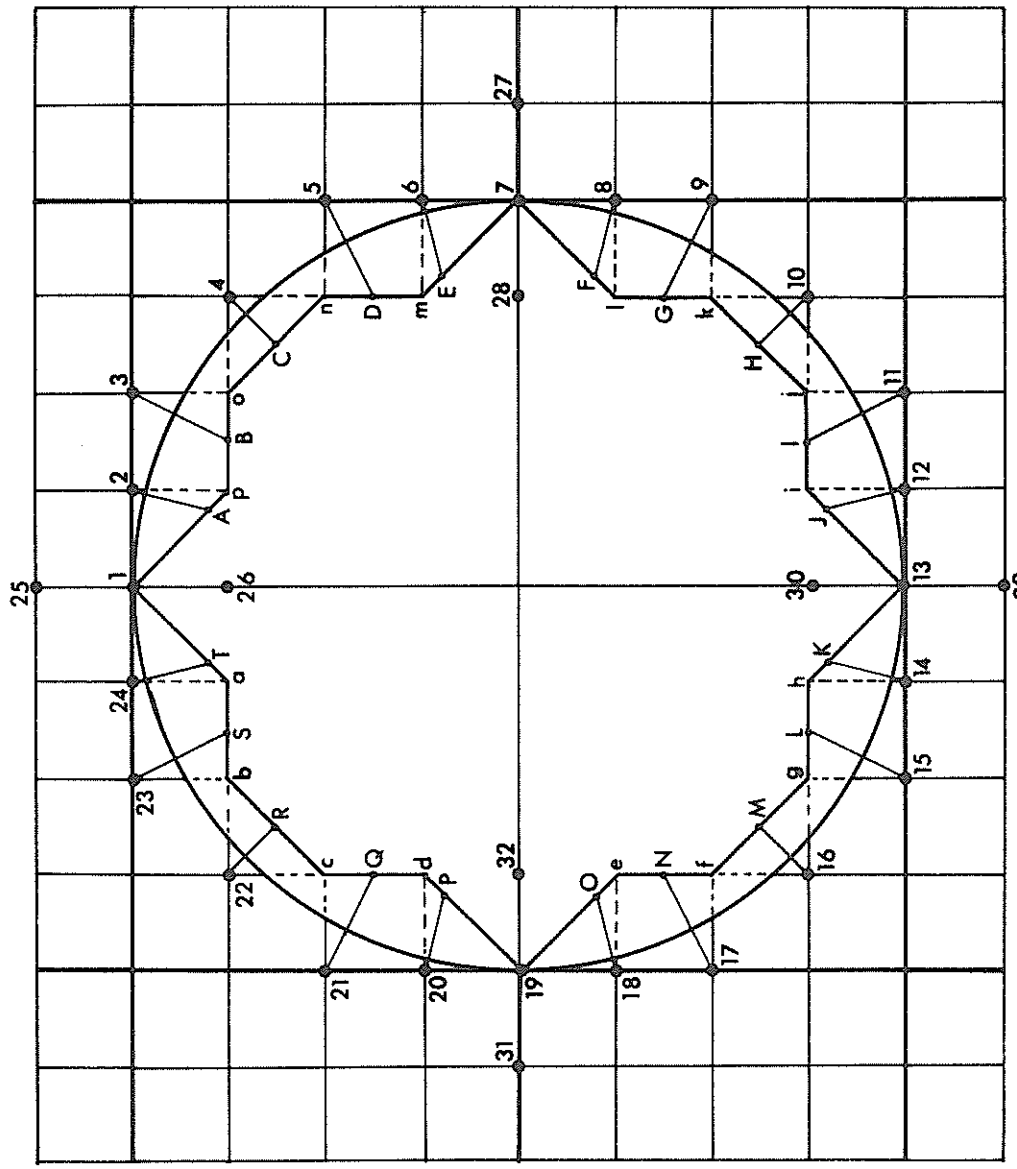

Fig. 4.6 — FINITE DIFFERENCE SCHEME ON CIRCULAR PIPE SURFACE

$$\frac{\partial p}{\partial n} = \frac{p_2 - p_A}{2A} = 0 \quad \ldots\ldots\ldots\ldots\ldots\ldots \quad (4.13)$$

or

$$p_A = p_2 \quad \ldots\ldots\ldots\ldots\ldots\ldots\ldots\ldots \quad (4.14)$$

Substituting p_A into Eq. 4.12 we obtain

$$p1\ (p_2) = Ap(p_1) + A1(p_p) \quad \ldots\ldots\ldots\ldots \quad (4.15)$$

Likewise

$$po(p_3) = Bo(p_p) + pB(p_o) \quad \ldots\ldots\ldots\ldots \quad (4.16)$$

$$on(p_4) - Cn(p_o) + oC(p_n) \quad \ldots\ldots\ldots\ldots \quad (4.17)$$

$$nm(p_5) = Dm(p_n) + nD(p_m) \quad \ldots\ldots\ldots\ldots \quad (4.18)$$

$$m7(p_6) = E7(p_m) + mE(p_7) \quad \ldots\ldots\ldots\ldots \quad (4.19)$$

so that equations can be written for all the irregular grid points around the pipe surface in terms of internal fictitious grid point values. Notice that one of the fictitious points in each equation is repeated in the next equation. Equations for points 1, 7, 13 and 19 can be written in terms of regular grid point values as if they were on a flat surface as in the last section. For example:

$$4p_1 = p_{24} + p_2 + 2p_{25} \quad \ldots\ldots\ldots\ldots\ldots \quad (4.20)$$

$$4p_7 = p_6 + p_8 + 2p_{27} \quad \ldots\ldots\ldots\ldots\ldots \quad (4.12)$$

By combining all the above equations, fictitious values can be eliminated by substitutions, and relations for pressure functions at grids points around the pipe can be developed in terms of neighboring

regular grid points.

Relaxation Method

The Laplace equation (Eq. 3.6) is an elliptic partial differential equation and can be solved by an iterative technique called the Relaxation Method. This is essentially an implicit difference method where the calculation of an unknown pivotal value necessitates the solution of a set of simultaneous equations. Consider the finite difference equation (Eq. 4.10) for any point (i, j)

$$p_{i,\,j} = \frac{(p_{i,\,j+1} + p_{i,\,j-1}) + ER(p_{i-1,\,j} + p_{i+1,\,j})}{2ER}$$

A set of equations can be written for the whole net work of grid points within the problem region of concern. By the Relaxation Method, unknown values in the $i+1^{th}$ row are specified in terms of known values in the i^{th} row by a single application of the above expression. If there are N unknown values in the $i+1^{th}$ row, the general equation above must be applied N times across the length of the row. The resulting system of N simultaneous equations specifies the N net values implicitly. The whole system of equations forms a tridiagonal matrix and is readily solved by a Gaussian Elimination Method if the boundary conditions of the problem region are known.

Successive-Over-Relaxation Method. We now consider an additional method called the Successive-Over-Relaxation Method (SOR)

which will accelerate convergence to the solution of the finite difference elliptic equation. This is again an iterative technique in which an improved estimate of the p value is computed by applying the following equation at every grid point:

$$\overline{p_{i,j}^{n+1}} = p_{i,j}^{n} + w(p_{i,j}^{n+1} - p_{i,j}^{n}) \quad \ldots\ldots\ldots \quad (4.23)$$

where $p_{i,j}^{n}$ is the p value at point (i,j) calculated after n iterations $p_{i,j}^{n+1}$ is the p value calculated after n+1 iterations and $\overline{p_{i,j}^{n+1}}$ is the improved new estimate by introducing the SOR factor w. The location of the optimum value of the parameter w is different for each individual problem and can be determined only by experimental trials. A good choice of w is found to be within the range $1<w<2$ for rapid convergence.

Exponential Extrapolation Method

Another method for accelerating convergence in the iterative procedure is called the Exponential Extrapolation Method. Fig. 4.7 shows a sketch of estimated p values plotted against their corresponding number of iterations. This is an exponential curve which levels off to the true value of p after an infinite number of iterations. p_n, p_{n-1} and p_{n-2} denotes the estimated p value after n^{th}, $n-1^{th}$ and $n-2^{th}$ iterations respectively. Δ_1 is the difference between p_n and p_{n-1}, and Δ_2 is the difference between p_{n-1} and p_{n-2}. It can be shown that a good approximate p value can be given by the following relation:

$$p = p^{n} - \left(\frac{\Delta_1^{\,2}}{\Delta_1 - \Delta_2}\right) \cdot \cdot \cdot \cdot \cdot \cdot \cdot \cdot \cdot \cdot \cdot \cdot \cdot \quad (4.24)$$

so that convergence in the Relaxation process can be achieved by skipping a large number of iterations.

Because of the large system of grid points encountered in this finite difference problem, these convergence accelerating techniques are vital in reducing the amount of computer time needed.

A computer program (12) based on the finite difference approach just developed was written to solve for the pressure distribution around a buried pipe. Results and usage of the program will be discussed in Chapter VI.

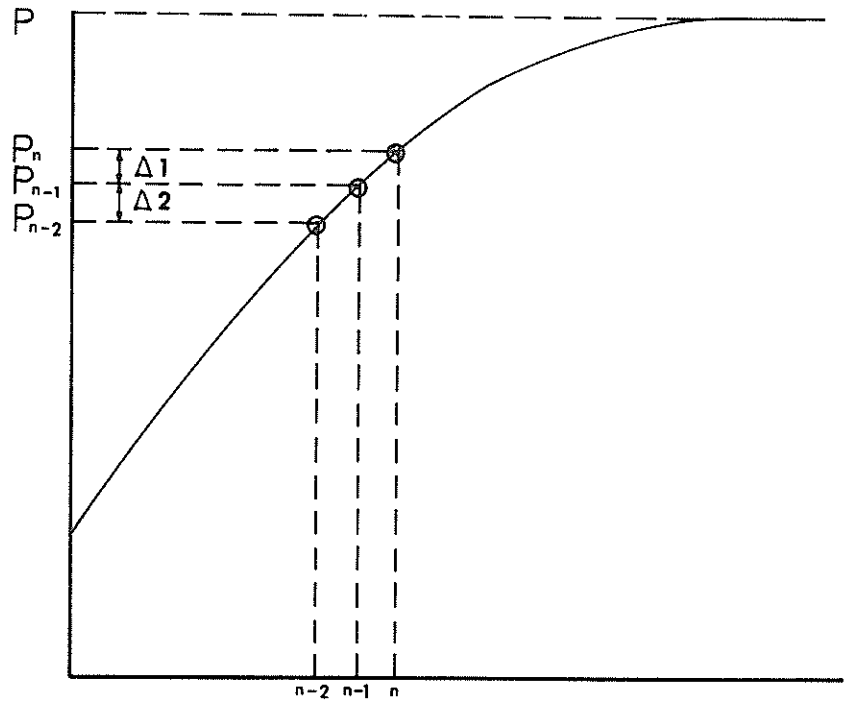

Fig. 4.7 - Exponential Extrapolation Scheme

CHAPTER V

FINITE ELEMENT APPROXIMATION

Principles of the Finite Element Method

The finite element method is essentially a process through which a continuum with infinite degrees of freedom can be approximated to by an assemblage of subregions (or elements) each with a specified but now finite number of unknowns. A variational, extremum approach, valid over the whole region of concern is used in this problem and the solution is the one minimizing some quantity I which is defined by suitable integration of the unknown quantities over the whole domain. I is a function of the unknown function p(x, y) and its derivatives, and is known as a "functional".

$$I(p) = \iint_S f(p, x, y, \frac{\partial p}{\partial x}, \frac{\partial p}{\partial y})\, dx\, dy \quad \ldots\ldots \quad (5.1)$$

The Euler-Langrange Theorem (22) states that if the above integral is to be minimized over a bounded region S, then the necessary and sufficient condition for this minimum to be reached is that the unknown function p(x, y) should satisfy the following differential equation

$$\frac{\partial f}{\partial p} - \frac{\partial}{\partial x}\left[\frac{\partial f}{\partial(\frac{\partial p}{\partial x})}\right] - \frac{\partial}{\partial y}\left[\frac{\partial f}{\partial(\frac{\partial p}{\partial y})}\right] = 0 \quad \ldots\ldots\ldots \quad (5.2)$$

within the same region, provided p satisfies the boundary conditions specified. It can be verified that the equivalent formulation to Eq. 5.2 is the requirement that the surface integral given below and taken over the whole region should be minimized

$$I = \iint_S \left\{ \frac{1}{2} \left[\left(\frac{\partial p}{\partial x}\right)^2 + \left(\frac{\partial p}{\partial y}\right)^2 \right] \right\} dx\, dy \quad \ldots\ldots\ldots \quad (5.3)$$

subject to p obeying the same boundary conditions.

The region under consideration is to be divided into subregions called elements, and the function which we are trying to determine can be described in each element as

$$p = \left[N \right] \left\{ p \right\}^e \quad \ldots\ldots\ldots\ldots\ldots \quad (5.4)$$

$\left\{p\right\}^e$ is a column matrix containing nodal values of the function associated with a single element as indicated by the superscript e. $\left[N\right]$ is a matrix containing the shape function of the co-ordinates. In order to minimize the functional I with respect to the total number of parameters $\left\{p\right\}$ associated with the whole domain, we must write a system of equations

$$\frac{\partial I}{\partial \left\{p\right\}} = \begin{Bmatrix} \frac{\partial I}{\partial p_1} \\ \frac{\partial I}{\partial p_2} \\ \vdots \end{Bmatrix} = 0 \quad \ldots\ldots\ldots\ldots \quad (5.5)$$

The total function is equal to the sum of the contributions

of each element, such that

$$I = \sum I^e \quad \ldots\ldots\ldots\ldots\ldots\ldots (5.6)$$

A typical equation then becomes

$$\frac{\partial I}{\partial p_n} = \sum \frac{\partial I^e}{\partial p_n} = 0 \quad \ldots\ldots\ldots\ldots\ldots (5.7)$$

with the summation taken over all the elements.

It can be shown that the element derivatives can be written in a linear form as

$$\frac{\partial I^e}{\partial \{p\}^e} = [E]^e \{p\}^e + \{F\}^e \quad \ldots\ldots\ldots (5.8)$$

in which $[E]$ and $\{F\}^e$ are matrices of constants.

Now the minimizing set of Eqs. 5.5 can be written as

$$\frac{\partial I}{\partial \{p\}} = [E]\{p\} + \{F\} = 0 \quad \ldots\ldots\ldots (5.9)$$

in which

$$[E_{i,j}] = \sum [E_{i,j}]^e \quad \ldots\ldots\ldots\ldots (5.10)$$

$$[F_{i,j}] = \sum [F_{i,j}]^e \quad \ldots\ldots\ldots\ldots (5.11)$$

with summation over all elements.

Formulation of Finite Element Method

Consider again the Laplace Equation (Eq. 3.6) in the problem

region shown in Fig. 5.2 subject to the prescribed value $p = p_b$ on the outer boundary and the normal derivative boundary condition $\frac{\partial p}{\partial n} = 0$ on the pipe surface inside the region. It can be mathematically shown by using the Euler-Lagrange Equation that this is equivalent to finding a function p which satisfies the boundary conditions and minimizes

$$I = \iint \left[\tfrac{1}{2}\left(\frac{\partial p}{\partial x}\right)^2 + \tfrac{1}{2}\left(\frac{\partial p}{\partial y}\right)^2 \right] dxdy \quad . \quad . \quad . \quad . \quad . \quad (5.12)$$

For the approximate solution we shall assume the region to be divided into finite elements (Fig. 14) in each of which

$$p = \left[N_i, N_j \ldots \right] \begin{Bmatrix} p_i \\ p_j \\ \vdots \end{Bmatrix} = \left[N \right] \left\{ p \right\}^e \quad . \quad . \quad . \quad . \quad (5.13)$$

where $\left\{ p \right\}^e$ represents a list of p values at the element nodes.

Assuming that p is continuous between elements, then Eq. 5.6 is satisfied and we can confine our attention to a typical element with node points (i, j, k) as in Fig. 5.1

p as a linear function in x and y

$$p = a + bx + cy \quad . \quad . \quad . \quad . \quad . \quad . \quad . \quad . \quad . \quad . \quad . \quad . \quad . \quad (5.14)$$

$$\left.\begin{aligned} p_i &= a + bx_i + cy_i \\ p_j &= a + bx_i + cy_j \\ p_x &+ a + bx_k + cy_k \end{aligned}\right\} \quad . \quad . \quad . \quad . \quad . \quad . \quad . \quad . \quad . \quad . \quad . \quad (5.15)$$

Combining contributions from all three node points of the triangular

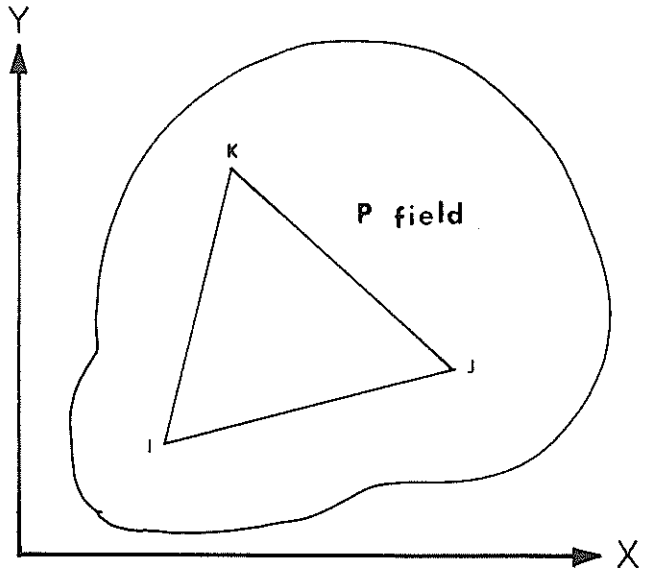

Fig. 5.1 - Typical Triangular Element

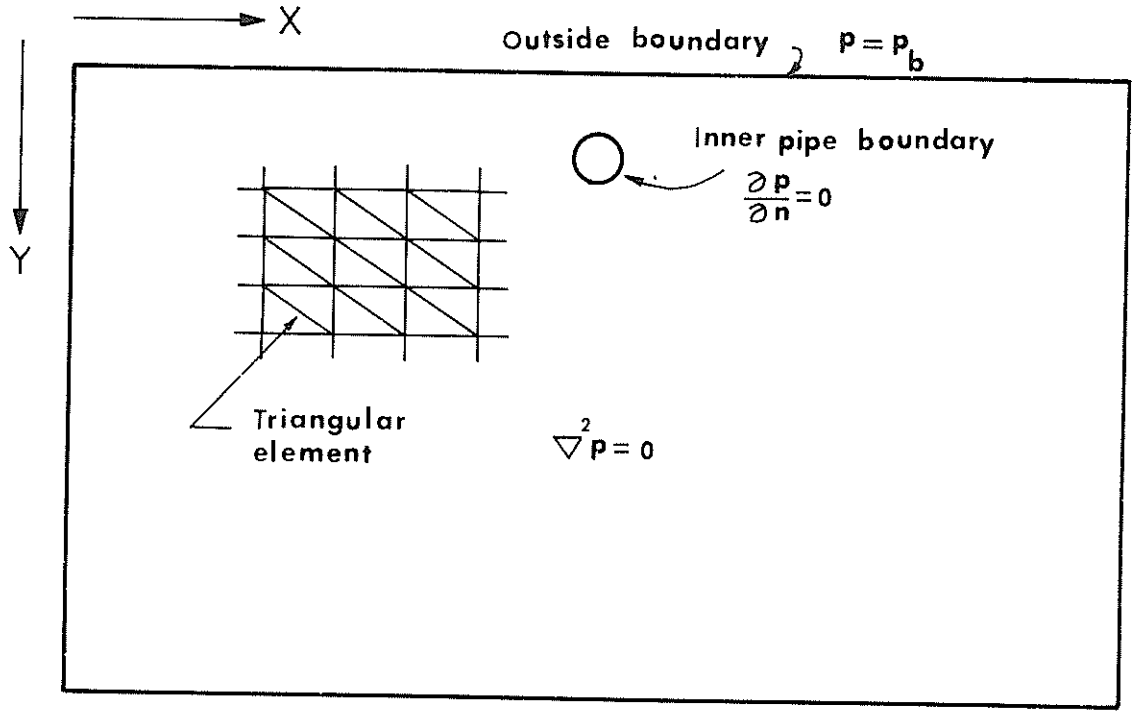

Fig. 5.2 - Problem Region of Finite Element System

element

$$p = \frac{1}{2A}\left[(a_i + b_i x + c_i y)p_i + (a_j + b_j x + c_j y)p_j + (a_k + b_k x + c_k y)p_k\right] \quad \ldots\ldots\ldots\ldots (5.16)$$

in which

$$A = \tfrac{1}{2} \det \begin{vmatrix} 1 & x_i & y_i \\ 1 & x_j & y_j \\ 1 & x_k & y_k \end{vmatrix} = \text{Area of triangular element} \quad \ldots (5.17)$$

and

$$\left.\begin{aligned} a_i &= x_j y_k - x_k y_j \,,\; b_i = y_j - y_k \,,\; c_i = x_k - x_j \\ a_j &= x_k y_i - x_i y_k \,,\; b_j = y_k - y_i \,,\; c_j = x_i - x_k \\ a_k &= x_i y_j - x_j y_i \,,\; b_k = y_i - y_j \,,\; c_k = x_j - x_i \end{aligned}\right\} \quad \ldots (5.18)$$

Differentiating p with respect to x and y gives

$$\frac{\partial p}{\partial x} = \frac{1}{2A}\begin{bmatrix} b_i & b_j & b_k \end{bmatrix}\begin{Bmatrix} p_i \\ p_j \\ p_k \end{Bmatrix} \quad \ldots\ldots\ldots\ldots (5.19)$$

$$\frac{\partial p}{\partial y} = \frac{1}{2A}\begin{bmatrix} c_i & c_j & c_k \end{bmatrix}\begin{Bmatrix} p_i \\ p_j \\ p_k \end{Bmatrix} \quad \ldots\ldots\ldots\ldots (5.20)$$

Again differentiating Eqs. 5.19 and 5.20 in the i, j, k directions separately

$$\left.\begin{aligned} \frac{\partial}{\partial p_i}\left(\frac{\partial p}{\partial x}\right) &= \frac{b_i}{2A} \\ \frac{\partial}{\partial p_j}\left(\frac{\partial p}{\partial x}\right) &= \frac{b_j}{2A} \\ \frac{\partial}{\partial p_k}\left(\frac{\partial p}{\partial x}\right) &= \frac{b_k}{2A} \end{aligned}\right\} \quad \ldots\ldots\ldots\ldots\ldots (5.21)$$

$$\left.\begin{aligned} \frac{\partial}{\partial p_i}\left(\frac{\partial p}{\partial y}\right) &= \frac{c_i}{2A} \\ \frac{\partial}{\partial p_j}\left(\frac{\partial p}{\partial y}\right) &= \frac{c_j}{2A} \\ \frac{\partial}{\partial p_k}\left(\frac{\partial p}{\partial y}\right) &= \frac{c_k}{2A} \end{aligned}\right\} \quad \ldots\ldots\ldots\ldots\ldots\ldots \quad (5.22)$$

From Eq. 5.12

$$\left.\begin{aligned} \frac{\partial I}{\partial p_i} &= \iint\left[\frac{\partial p}{\partial x}\cdot\frac{\partial}{\partial p_i}\left(\frac{\partial p}{\partial x}\right) + \frac{\partial p}{\partial y}\cdot\frac{\partial}{\partial p_i}\left(\frac{\partial p}{\partial y}\right)\right] dxdy \\ \frac{\partial I}{\partial p_j} &= \iint\left[\frac{\partial p}{\partial x}\cdot\frac{\partial}{\partial p_j}\left(\frac{\partial p}{\partial x}\right) + \frac{\partial p}{\partial y}\cdot\frac{\partial}{\partial p_j}\left(\frac{\partial p}{\partial y}\right)\right] dxdy \\ \frac{\partial I}{\partial p_k} &= \iint\left[\frac{\partial p}{\partial x}\cdot\frac{\partial}{\partial p_k}\left(\frac{\partial p}{\partial x}\right) + \frac{\partial p}{\partial y}\cdot\frac{\partial}{\partial p_k}\left(\frac{\partial p}{\partial y}\right)\right] dxdy \end{aligned}\right\} \quad (5.23)$$

Substituting $\frac{\partial I}{\partial p}$ and $\frac{\partial^2 I}{\partial p^2}$ into Eq. 5.23, the following matrix equation is obtained.

$$\frac{\partial I}{\partial p} = \begin{Bmatrix} \frac{\partial I}{\partial p_i} \\ \frac{\partial I}{\partial p_j} \\ \frac{\partial I}{\partial p_k} \end{Bmatrix} = \frac{1}{4A}\begin{bmatrix} b_i b_i & b_i b_j & b_i b_k \\ b_j b_i & b_j b_j & b_j b_k \\ b_k b_i & b_k b_j & b_k b_k \end{bmatrix}\begin{Bmatrix} p_i \\ p_j \\ p_k \end{Bmatrix} +$$

$$\frac{1}{4A}\begin{bmatrix} c_i c_i & c_i c_j & c_i c_k \\ c_j c_i & c_j c_j & c_j c_k \\ c_k c_i & c_k c_j & c_k c_k \end{bmatrix}\begin{Bmatrix} p_i \\ p_j \\ p_k \end{Bmatrix} \quad \ldots\ldots \quad (5.24)$$

or

$$\frac{\partial I}{\partial p} = \frac{1}{4A} \begin{bmatrix} b_i b_i + c_i c_i & b_i b_j + c_i c_j & b_i b_k + c_i c_k \\ b_j b_i + c_j c_i & b_j b_j + c_j c_j & b_j b_k + c_j c_k \\ b_k b_i + c_k c_i & b_k b_j + c_k c_j & b_k b_k + c_k c_k \end{bmatrix} \begin{Bmatrix} p_i \\ p_j \\ p_k \end{Bmatrix} \quad (5.25)$$

Thus for each element

$$\left\{\frac{\partial I}{\partial p}\right\}^e = \left[E\right]\left\{p\right\}^e \quad \ldots\ldots\ldots\ldots\ldots\ldots (5.26)$$

This is the same equation as Eq. 5.8 except that $\left\{F\right\}^e$ is taken to be zero in our problem. $\left[E\right]$ thus formed is called the Element Stiffness Matrix (ESM).

By summing up all the elemental contributions

$$\left\{\frac{\partial I}{\partial p}\right\} = \sum \left[E\right] \left\{p\right\}^e = 0 \quad \ldots\ldots\ldots\ldots\ldots (5.27)$$

a Global Stiffness Matrix (GSM) is formed.

$$\frac{\partial I}{\partial p} = \left[GSM\right]\left\{p\right\} = 0 \quad \ldots\ldots\ldots\ldots\ldots (5.28)$$

The above equation is then solved by the Gaussian Elimination Method.

Boundary Condition Considerations

Boundary conditions for the problem of interest can be divided into two cases (Fig. 5.3).

(i) a boundary with the value of p specified

$$p = p_b \quad \ldots\ldots\ldots\ldots\ldots\ldots (5.29)$$

(ii) an impermeable boundary with the normal derivative condition

$$\frac{\partial p}{\partial n} = 0 \quad \ldots\ldots\ldots\ldots\ldots\ldots\ldots \quad (5.30)$$

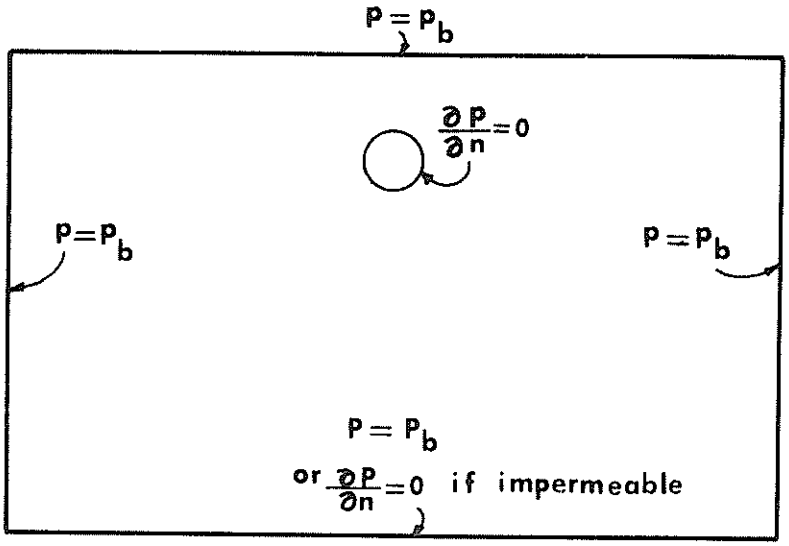

Fig. 5.3 - Boundary Conditions

A type (i) boundary condition is utilized on the outer boundaries of the rectangular region. Their specified values can be obtained from Liu's analytical equation as before (see Chapter III), and can easily be implemented in the finite element solution by making modifications in the Global Stiffness Matrix.

The type (ii) boundary condition exists on the pipe surface and the bottom boundary of the problem region if an impermeable layer is encountered, and therefore belongs to a general category

of derivative boundary conditions

$$\frac{\partial p}{\partial y} + ap + b = 0 \quad \ldots\ldots\ldots\ldots\ldots\ldots \quad (5.31)$$

in which a and b are constants. The implementation of this type of boundary condition in the finite element solution involves adding to the functional of Eq. 5.12 another integral pertaining to the boundary surface which, on minimization, automatically yields the boundary condition. In the general context by the Euler-Lagrange Equation this integral is simply

$$\int_S (qp + \tfrac{1}{2}\alpha p^2)\, ds \quad \ldots\ldots\ldots\ldots\ldots\ldots \quad (5.32)$$

in which S is the surface wave condition (ii) applies, and q and α are constants. Upon minimization, the contribution from this integral for each boundary element is found to be

$$\begin{bmatrix} 0 & 0 & 0 \\ 0 & \frac{\alpha\ell}{3} & \frac{\alpha\ell}{6} \\ 0 & \frac{\alpha\ell}{6} & \frac{\alpha\ell}{3} \end{bmatrix} \begin{Bmatrix} p_i \\ p_j \\ p_k \end{Bmatrix} + \begin{Bmatrix} 0 \\ \frac{q\ell}{2} \\ \frac{q\ell}{2} \end{Bmatrix} \quad \ldots\ldots\ldots \quad (5.33)$$

and must be added to the Element Stiffness Matrix during formulation. (i, j, k) are the node points of the triangular element, and ℓ is the length of one side of the element which constitutes the boundary of interest. However, in our problem, a and b in Eq. 5.31 are equal to zero. In such a case, α and q would also be zero thus canceling out the contribution of Eq. 5.33. This greatly simplifies the

solution of the problem because no additional consideration is needed for the normal derivative boundary condition, and Eq. 5.30 can be automatically satisfied without specifying values at the boundary points.

System of Finite Elements

In this study, elements of triangular shape are used. These elements can be graded in shape and size to follow arbitrary boundaries and to allow for regions of rapid variation of the function sought. Fig. 5.4 shows how the rectangular flow region can be subdivided into finite elements. In this figure, essentially two systems of triangular elements are utilized - an outer region of regular-sized elements and an inner region of finer, irregular-sized elements immediately surrounding the pipe. Fig. 5.5 is an enlargement of the inner region around a square pipe, an area where our interest is mainly concentrated. As for a circular pipe, its curved boundary can be approximated by small triangular elements constituting a multi-sided polygon as shown in Fig. 5.6. The size and number of these inner elements is determined by the accuracy required in the problem. Different systems of elements can be designed for the region depending on the size of the pipe and its depth of burial specified. One thing should be kept in mind, however, that elements of regular shape and size should be utilized as much as possible so that an automatic generation of elements for the region by the computer itself is possible.

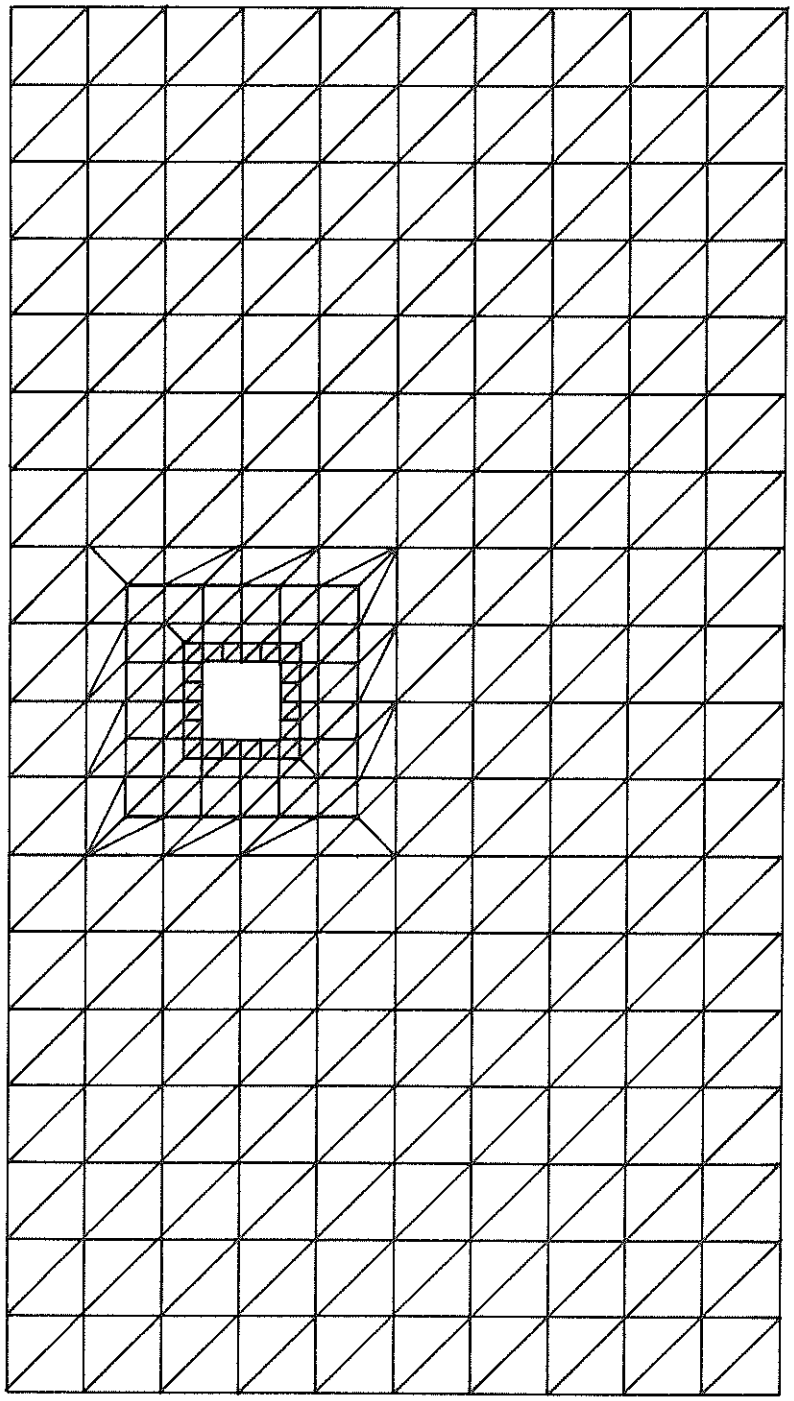

Fig. 5.4 - Finite Elements around a Square Pipe
(Solution Region)

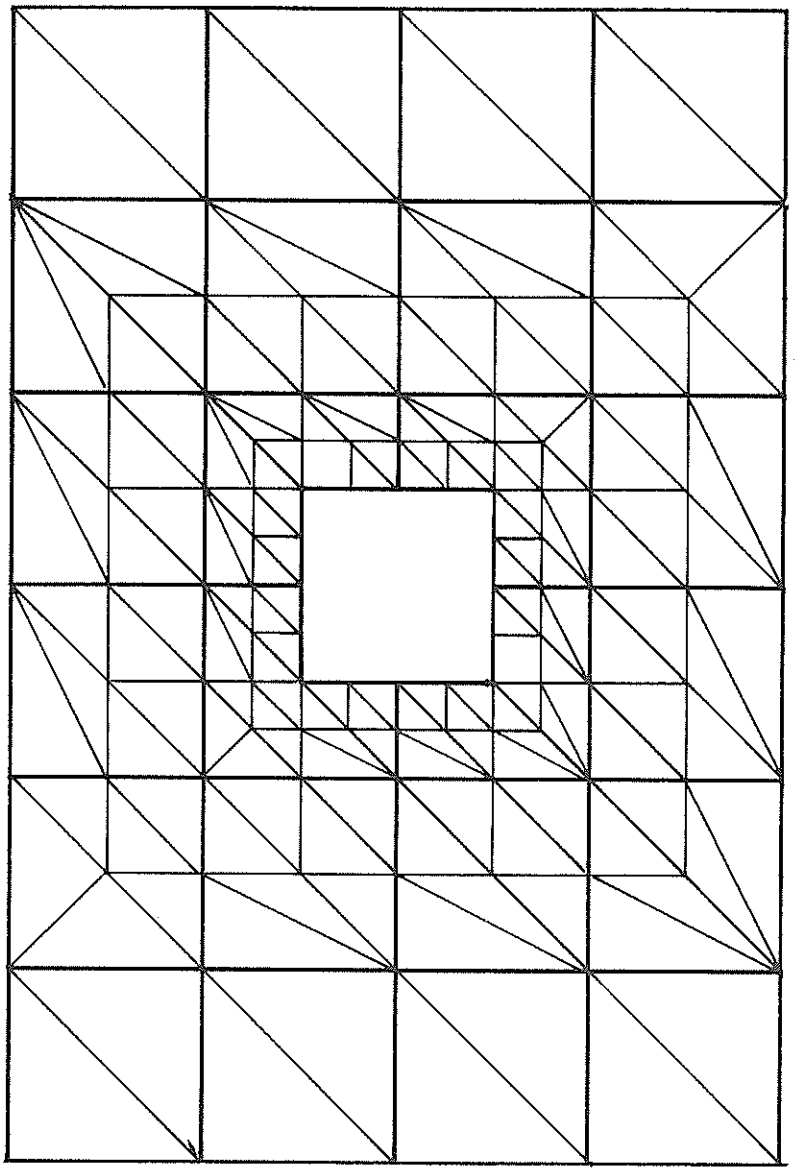

Fig. 5.5 - Finite Elements around a Square Pipe (inner region)

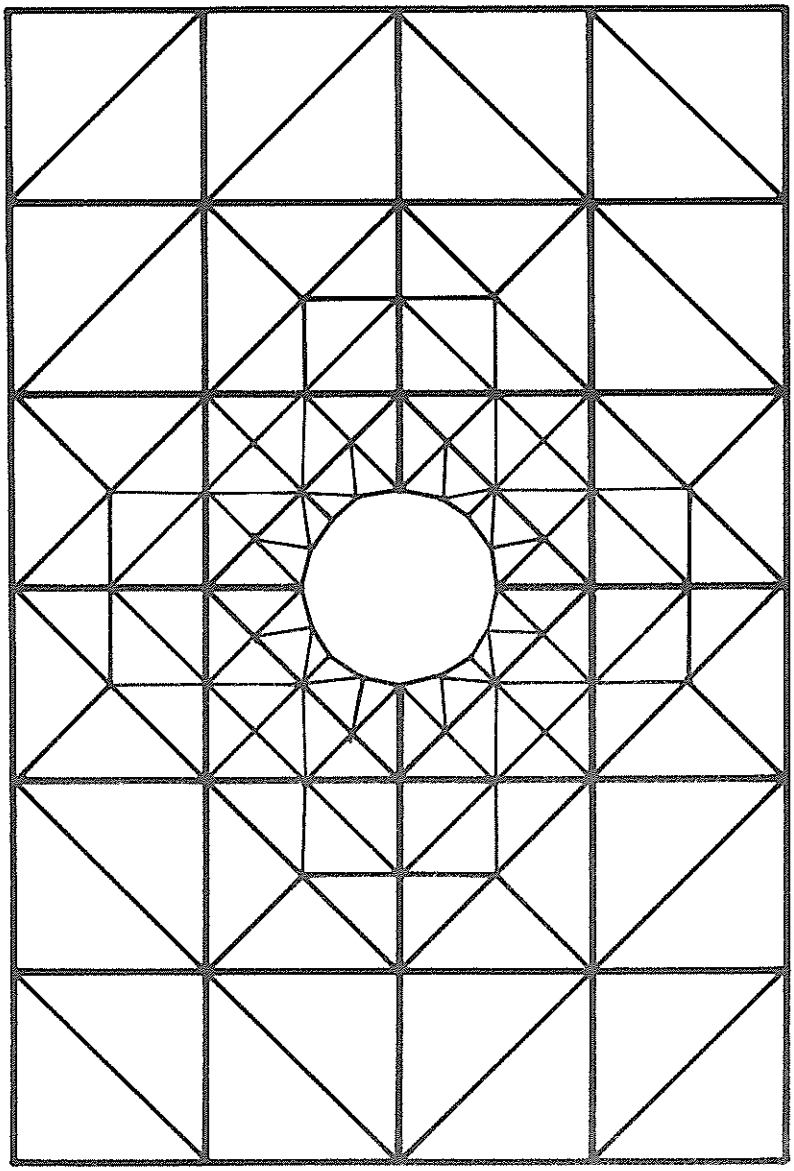

Fig. 5.6 — FINITE ELEMENTS AROUND A CIRCULAR PIPE

A computer program (11) based on the finite element approach just described was written to solve the pressure distribution problem. Results and usage of the program will be discussed in the next chapter.

CHAPTER VI

SOLUTION DEVELOPMENT AND RESULTS

Validation of Numerical Solutions

As part of this study, a validation check of the finite difference and finite element models with existing analytical and experimental results was undertaken. Its purpose was to test the accuracy of the numerical models, the solution schemes and the computer coding before they were applied to determine the dynamic pressure distribution that exist about a buried pipeline in a later section of this chapter.

Analytical results were available for the dynamic wave pressure distribution in the soil without a buried object in the region. Notable are Liu's (13) and Sleath's (20) studies previously discussed in Chapter III. An experimental study of the pressure distribution around a buried pipe was conducted by Campbell (7) as an integral part of this overall project. Dynamic wave pressure refers to the pressure fluctuation produced by a surface wave form with respect to the still water hydrostatic pressure as shown in Fig. 6.1. In this study, a perfectly drained condition was assumed in the soil region so that the dynamic pressure variation in the soil is completely in phase with the surface wave profile. As shown in Fig. 6.1, there is an increase of pressure under the crest and a decrease under the trough with respect to the normal hydrostatic pressure. This dynamic

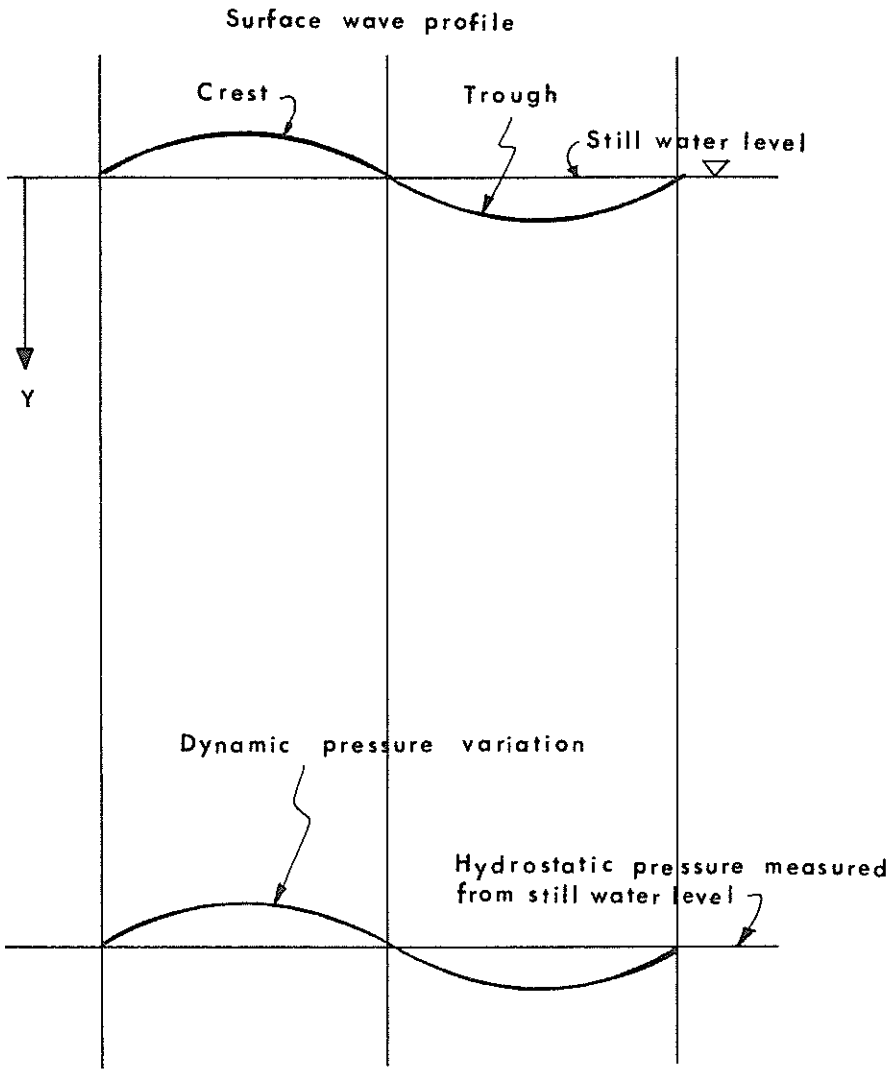

Fig. 6.1 - Dynamic Pressure Variation under a Surface Wave

pressure evaluated at a point in the soil region when added to the hydrostatic pressure will give the pore water pressure at that point.

Fig. 6.3 shows the damping effect on the dynamic pressure with depth, and is plotted at several points across the surface wave profile. It can be observed that the damping rate is greater in the soil that in the upper fluid medium. The maximum dynamic pressure appears directly under the crest or trough of the wave. The critical arrangement of wave and pipe positions which give this maximum pressure effect is shown in Fig. 6.2 with the pipe placed directly under the crest of the wave.

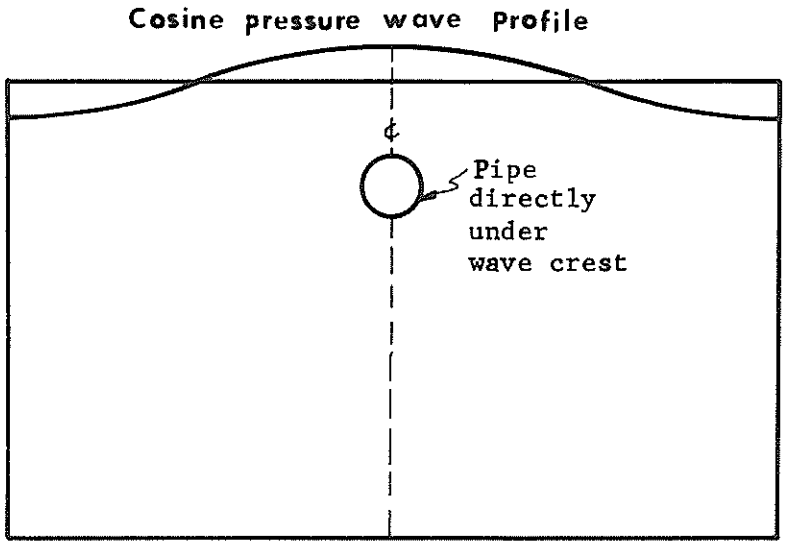

Fig. 6.2 - Critical Arrangement of Wave and Pipe Position

Finite Difference Model

In Liu's solution for determining the pressure distribution in the soil region, he assumed an infinite depth for the soil medium. His result as plotted in Fig. 3.3 shows that pressure values will be

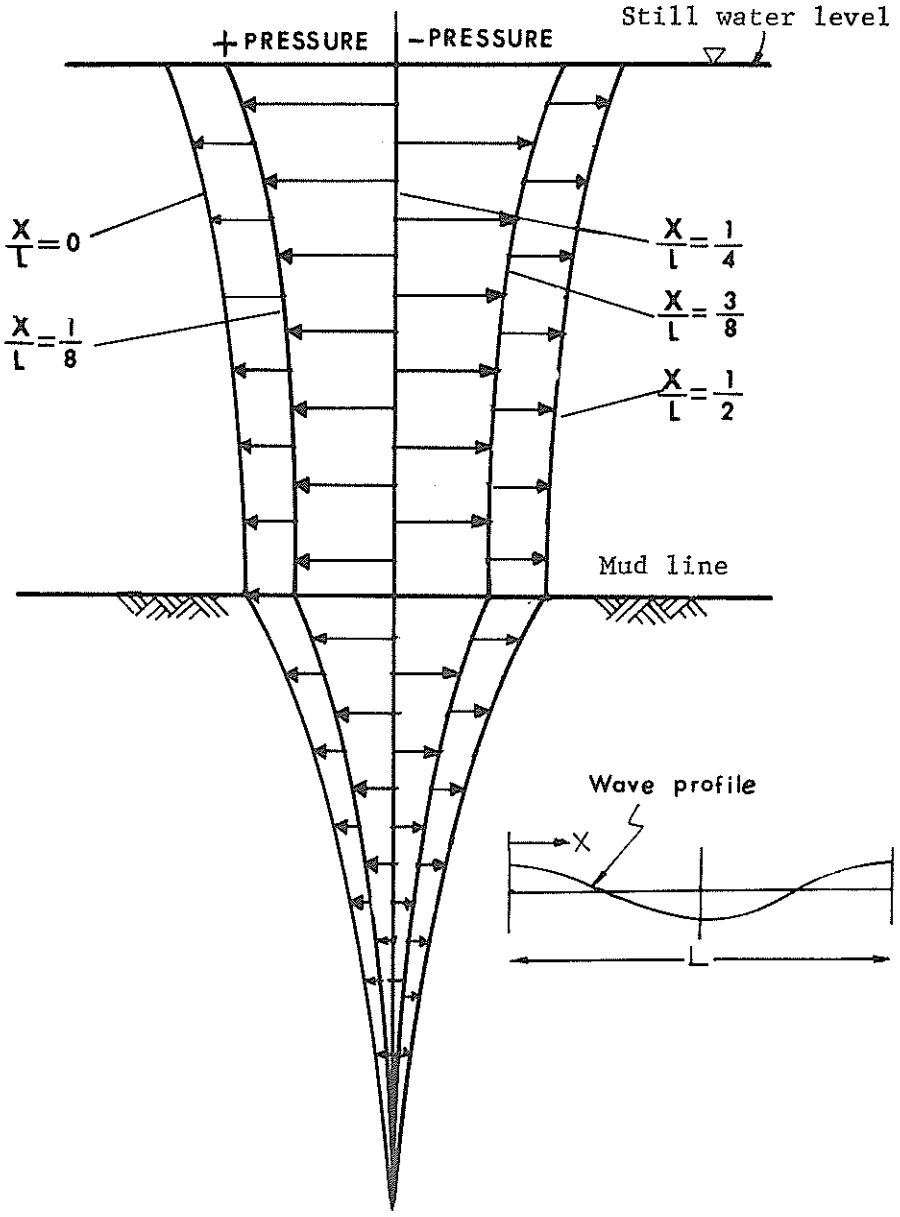

Fig. 6.3 - Damping of Dynamic Wave Pressure with Depth

damped to nearly zero at about one wave length below the mudline. In order to make comparisons between Liu's solution and the finite difference results, a square region with sides equal to one wave length was utilized in the finite difference scheme, and a zero dynamic pressure value is specified as a bottom boundary condition in the square region.

Eq. 3.6 was solved by the finite difference relaxation scheme with boundary values specified by choosing arbitrary wave and soil characteristics. This was then compared to Liu's results. It was found that the numerical solution depends on the grid size chosen in the problem region. A tendency to overpredict the pressure function when the grid spacings were too large and vice versa when the grid spacings were too small was found. Fig. 6.4 shows a plot of the various solutions using different grid sizes together with Liu's solution curve for the same wave and soil parameters. In this figure, SOR stands for Successive-Over-Relaxation approach. It can be seen that the solutions with grid sizes of 33 x 33 and 37 x 37 were almost identical to Liu's curve. It appears that an optimum value for the grid size does exist, and the solution generated by using that particular grid size will compare well with Liu's results. Fig. 6.5 illustrates the same effect by plotting different results against different grid sizes. From this study, it was concluded that the optimum grid size for the problem of interest is 37 x 37. As a result, this particular grid size was utilized throughout the finite difference study, with the assumption that it can be applied for all

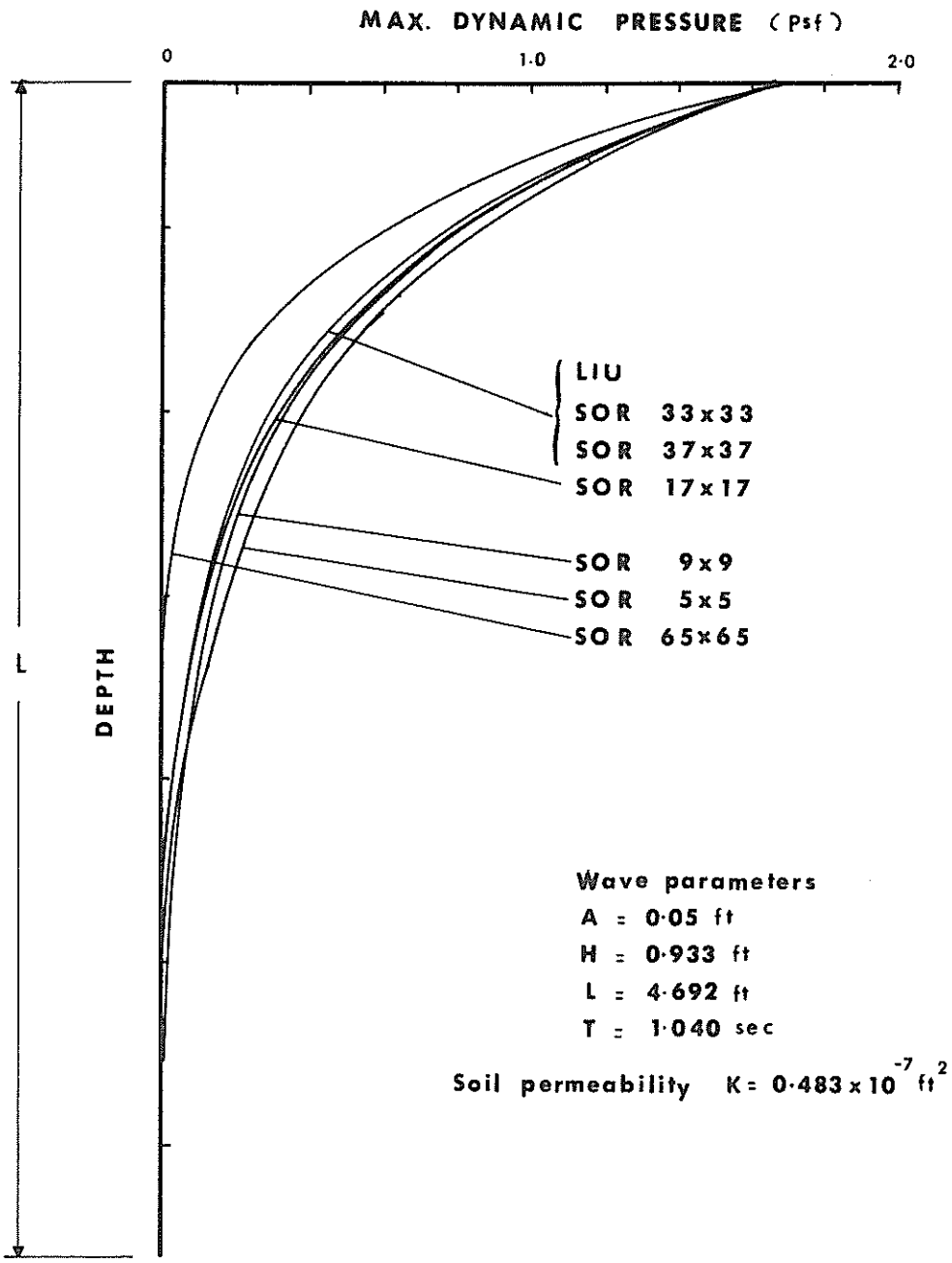

Fig. 6.4 - Relaxation Values by using Different Grid Sizes

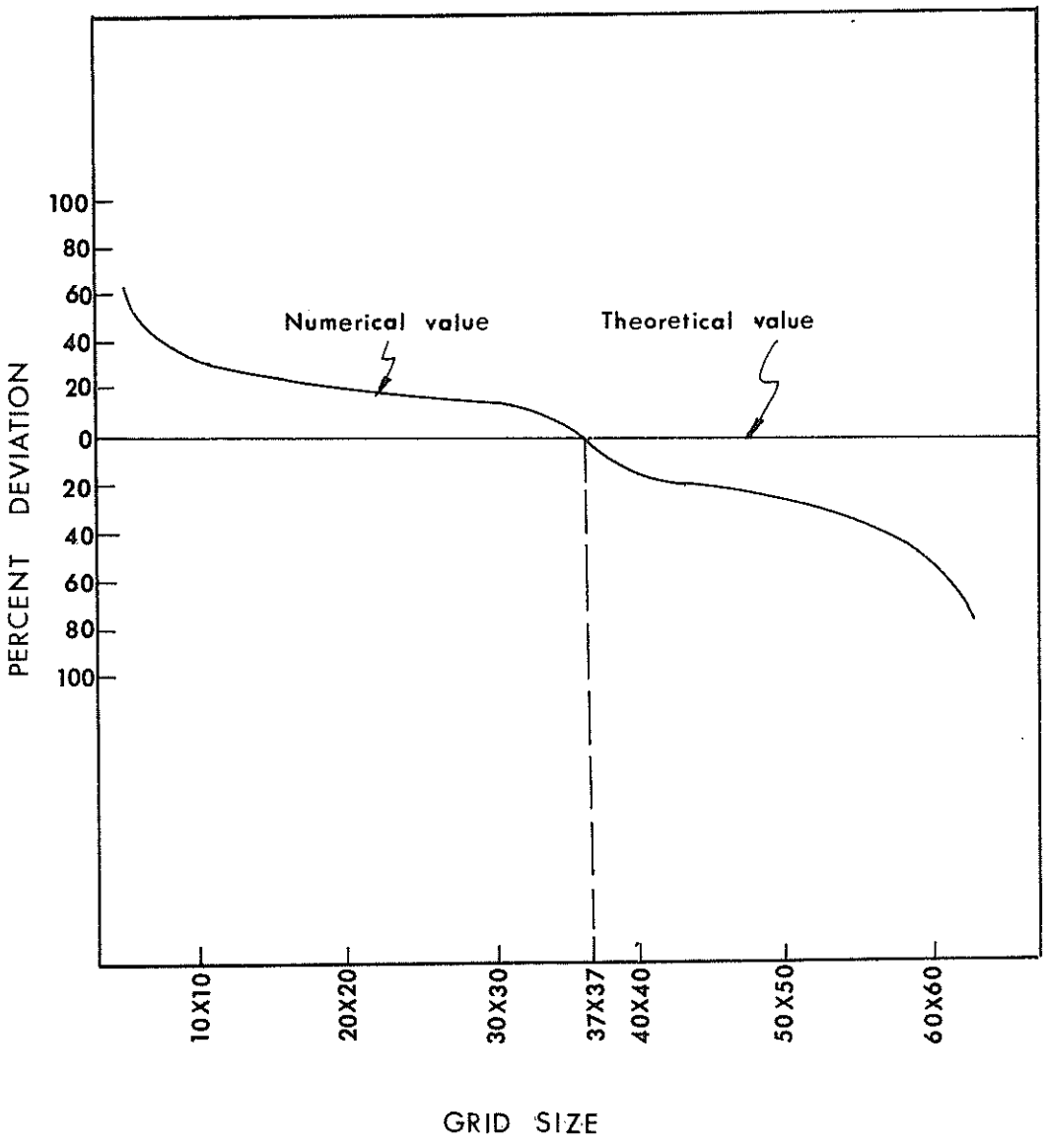

Fig. 6.5 - Grid size VS. Accuracy (Relaxation Method)

situations, including the placement of a pipe in the problem region.

The set of finer grids immediately surrounding the pipe was formed by subdividing from the regular 37 x 37 grid system such that their values can be readily obtained by a Linear Interpolation Method.

Finite Element Model

In checking the validity of the finite element model, a square region with simple triangular elements and sides equal to one wavelength as shown in Fig. 6.6 was first used. A study of the grid size effect showed that this model is less sensitive than the finite difference model. Better results were generally obtained with finer elements. However, due to a limited computer memory space, a grid system of 19 x 19 as shown in Fig. 6.6 was utilized. Zero value bottom boundary conditions were again specified, and results were obtained and compared to Liu's analytical solution. Fig. 6.7 is a plot showing four cases of pressure distribution in the soil region by using wave and soil parameters listed in Table 6.1.

Table 6.1 - Wave and Soil Parameters I

Case	1	2	3	4
H (in.)	3.2	2.0	1.0	0.5
T (sec.)	1.19	1.09	1.48	1.62
L (ft.)	4.5	4.0	6.17	6.25
h (ft.)	0.5	0.5	0.5	0.5
K ($ft.^2$)	5.62×10^{-10}	5.62×10^{-10}	5.62×10^{-10}	5.62×10^{-10}

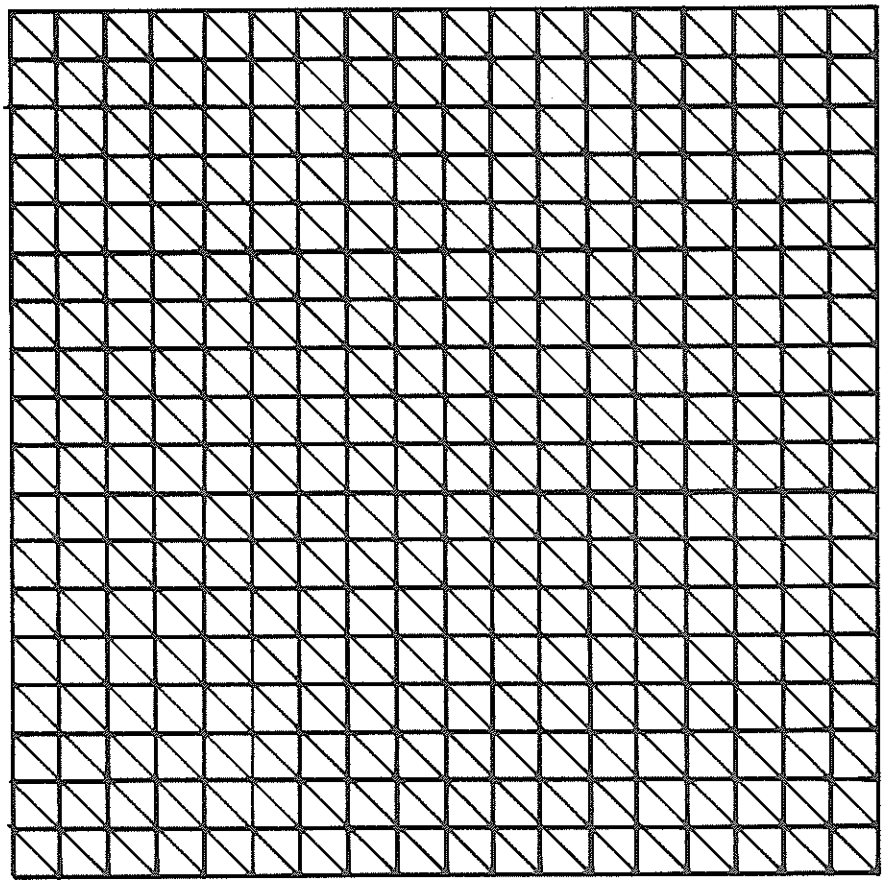

Fig. 6.6 - Finite Element Mesh System

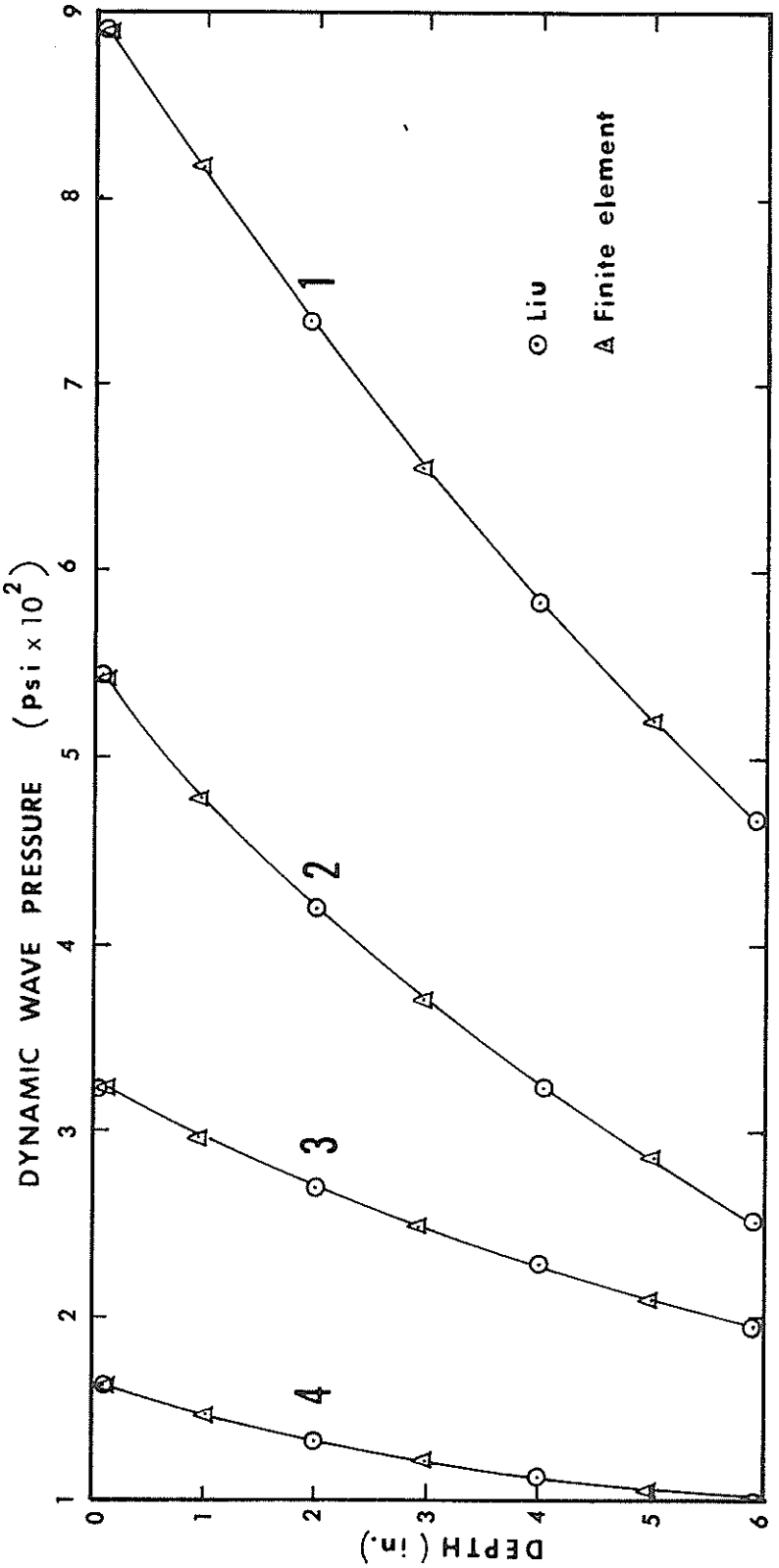

Fig. 6.7 - Comparison of Finite Element Method with Liu's Analytical Solution

Comparisons between the finite element and Liu's results show excellent agreement for all four cases. It can be concluded that the finite element model would give results as least as good as Liu's results. In addition, it can be modified to suit other situations as well.

In order to compare the numerical model results with experimental results generated by a wave-tank study (7), a slight modification had to be applied to the bottom boundary. In the wave-tank experiment, a soil depth of six inches was used, and the dynamic pressure distribution was expected to be affected by the presence of the impervious bottom of the tank. Modifications of the finite element region were necessary to simulate this impervious bottom boundary in the numerical model. The height of the problem region was shortened to an equivalent soil depth of six inches. Fig. 6.8 shows four cases of the pressure distribution measured in the soil along with the finite element results. As seen, curves obtained from the finite element model were shifted to the right of the experimental results. Better agreement is evident for the curves corresponding to the smaller waves. It is believed that this shifting was largely due to the difference in the top boundary values appearing in the two approaches. In the experimental study, small sand ripples were formed on the bottom during the course of pressure measurements. This irregularity might have caused some difference in the interface pressure values from those analytically predicted by liu's solution which assumes a horizontal sea bottom. However, judging from the shape of the curves, solutions obtained by

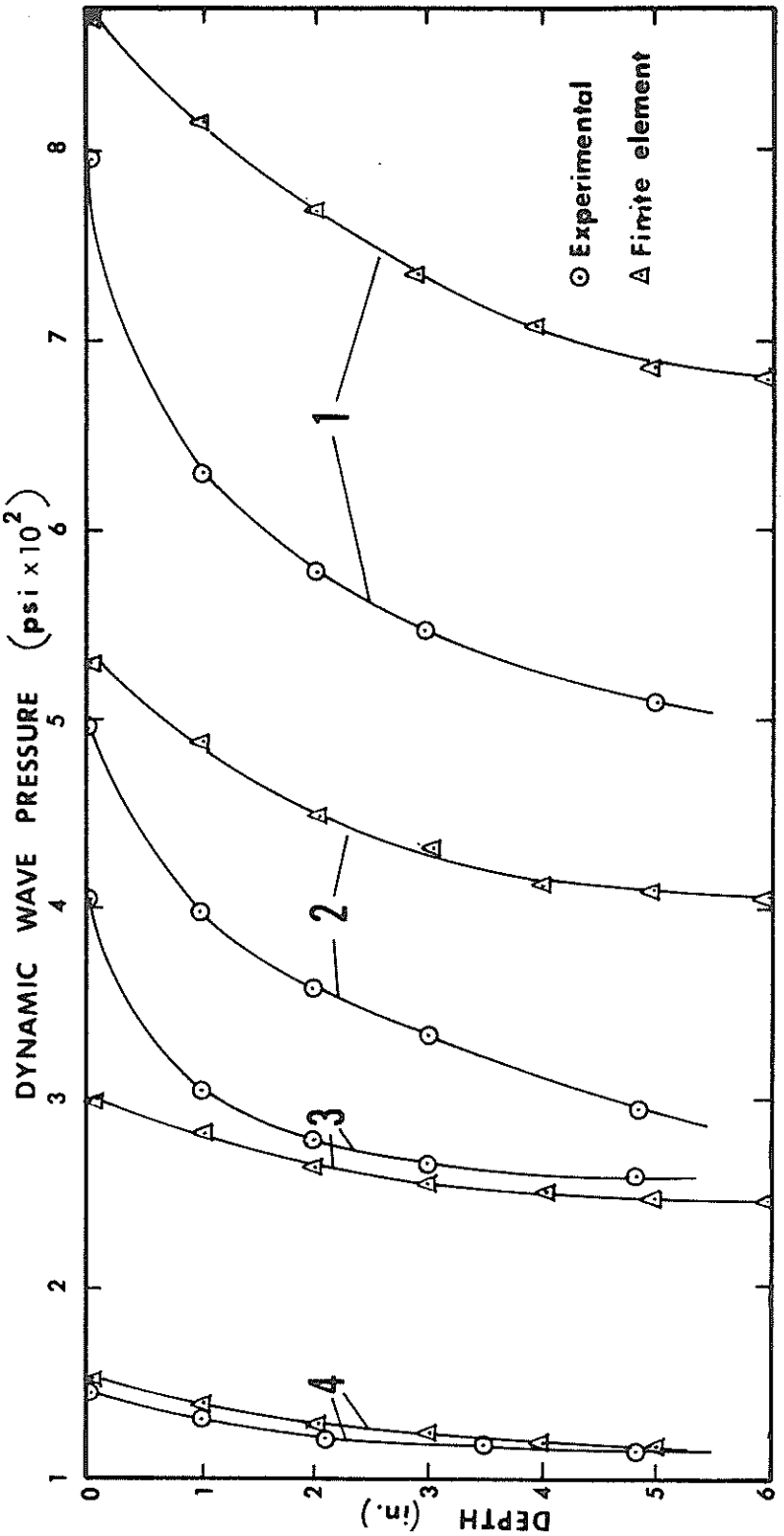

Fig. 6.8 - Comparison of Finite Element Method with Experimental Results

both methods follow much the same damping pattern. Better agreement could be achieved if actual, measured, boundary values were used as input in the finite element model instead of using Liu's analytical relations.

Pressure Distribution Pattern Around Buried Pipes

For demonstration purposes, a square pipe along with a circular pipe is considered in both the finite difference and finite element method solution.

Finite Difference Model

A square region with an embedded pipe (see Figs. 4.2 and 4.3) was first considered in this model. The input wave and soil parameters are as shown in Table 6.2:

Table 6.2 - Wave and Soil Parameters II

H (in.)	T (sec.)	L (ft.)	h (ft.)	K ($ft.^2$)
1.2	1.04	4.69	11.2	4.83×10^{-8}

The finite difference computer program (12) was first applied to a circular pipe with a diameter equal to L/18. The center of the pipe was located at a depth of 2.5 pipe-diameters below the mud line and at the center of the problem region. A wave profile position type (i) at the time instant t = 0 (Fig. 3.4) was specified on the interface boundary, and the bottom boundary values were taken to be

zero. The resulting computer output provided pressure values at all grid points in the problem region around the pipe.

Pressure values along the circular pipe surface are plotted in Fig. 6.9. Also plotted are initial pressure values existing in the soil sediment before the pipe was embedded in the region. A comparison of the two curves shows the effect of the introduction of the embedded pipe on the pressure distribution immediately surrounding the pipe. A slight increase of pressure (about 10%) at the top of the pipe and a decrease (about 20%) at the bottom of the pipe can be noted.

A square pipe with sides equal to L/18 and located at the same depth was considered next. The same boundary conditions and wave profile position as above were applied and results are plotted in Fig. 6.10. In this case, a more pronounced effect was observed in the pressure changes around the pipe, most probably due to the existence of sharp edges of the pipe. The results show an increase of about 40% at the top surface and a decrease of about 30% at the bottom. This same result can be seen in Fig. 6.11 in which pressure values are plotted along the center line A-B as shown. The boundary condition $\frac{\partial p}{\partial n} = 0$ on the pipe surface also appears in the resulting curve. The change of pressure along a vertical face of the square pipe is shown in Fig. 6.12.

In order to find the maximum effect under a progressive surface, a dynamic situation was simulated by moving the surface wave profile as if it were progressing with time (see Fig. 3.4), and results are

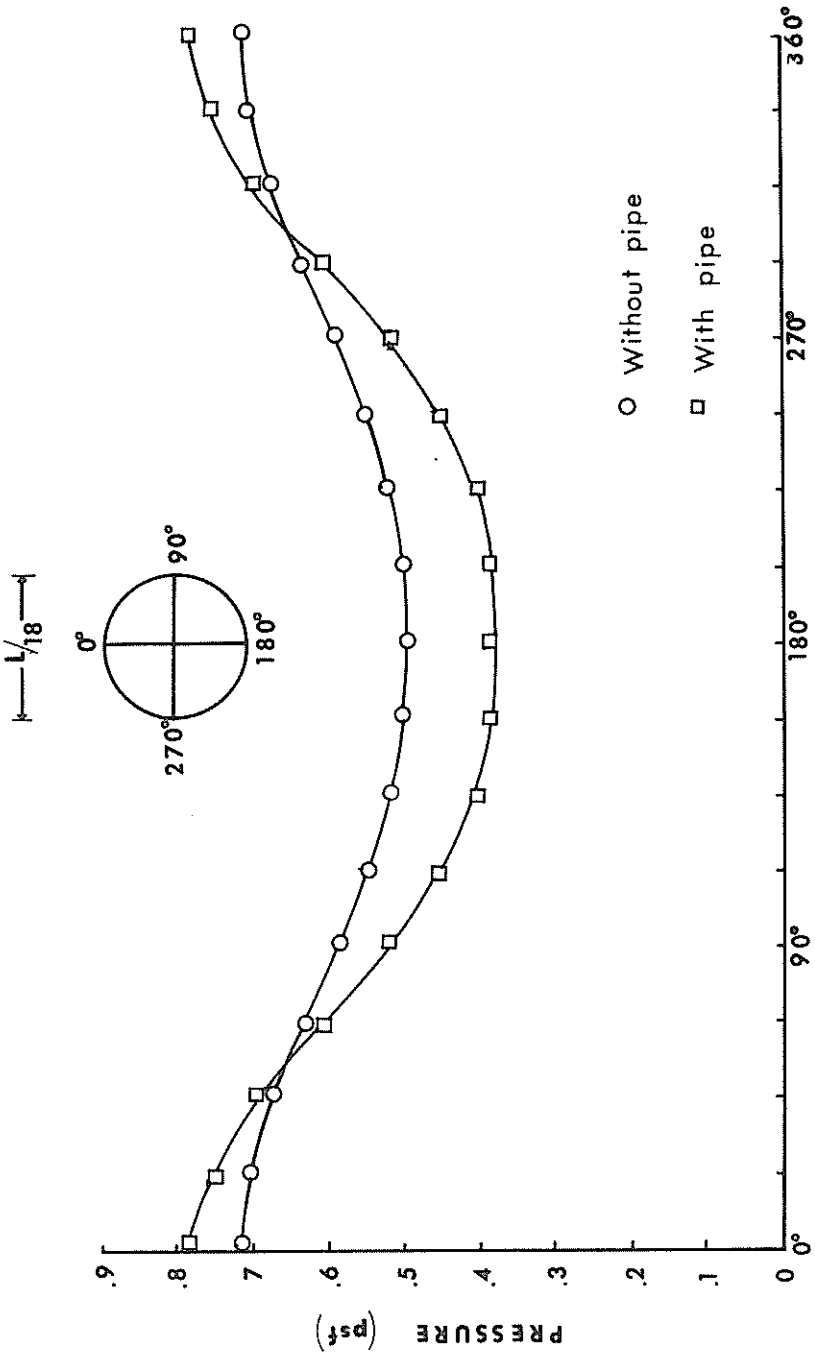

Fig. 6.9 - Pressure around a Circular Pipe at t = 0
(Finite Difference Method)

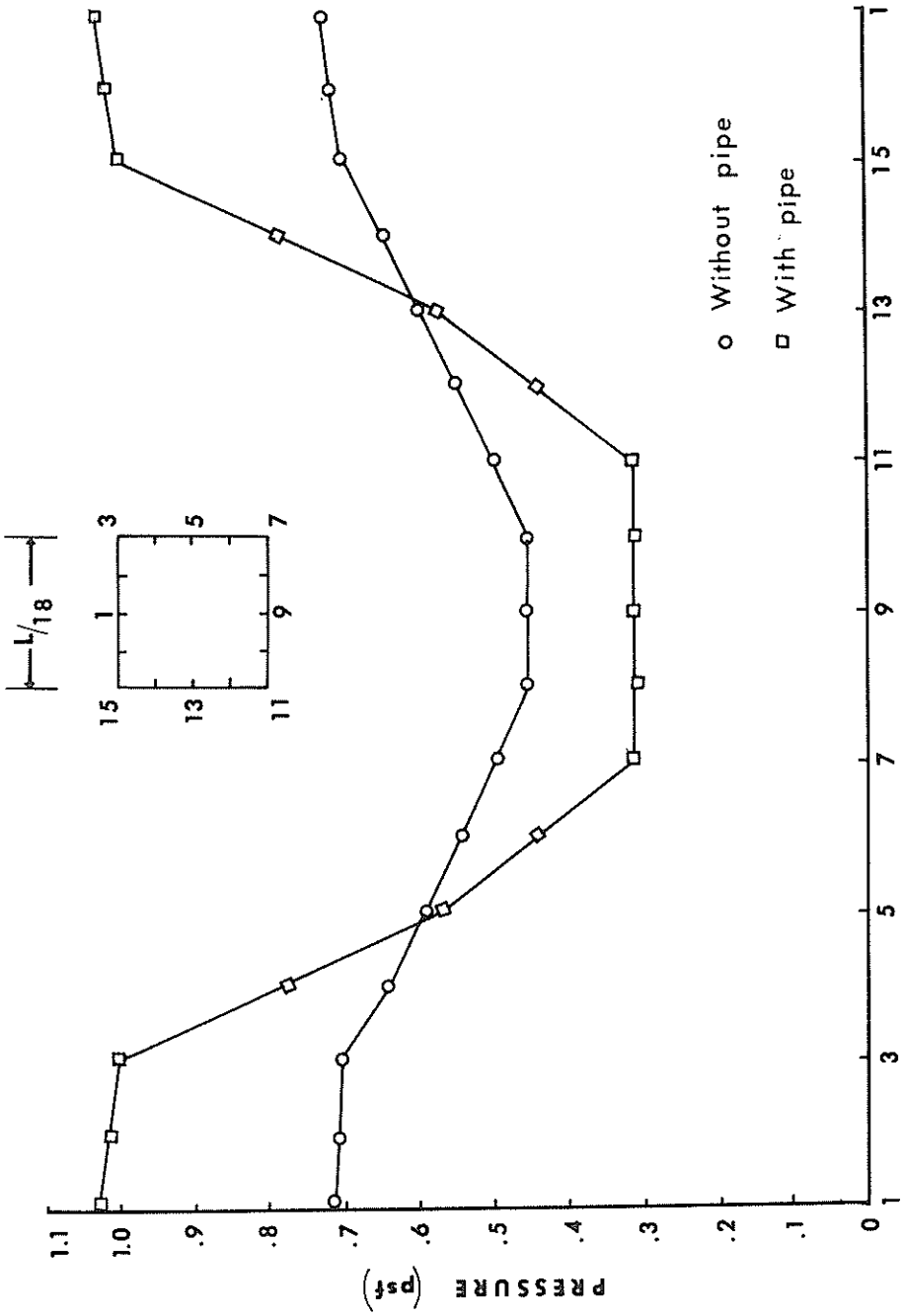

Fig. 6.10 - Pressure around a Square Pipe at t = 0
(Finite Difference Method)

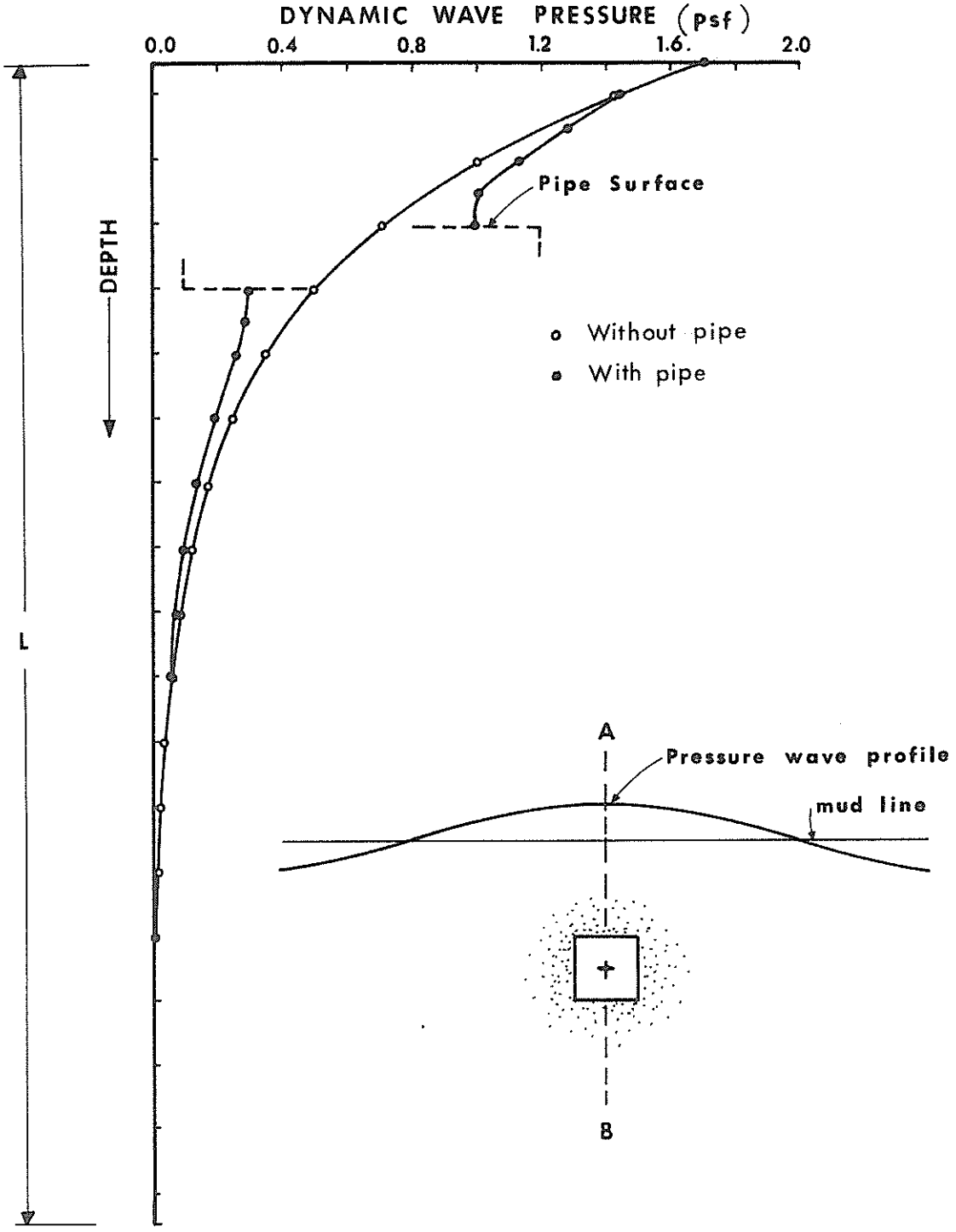

Fig.6.11– EFFECT OF PIPE ON PRESSURE IN SOIL ALONG A-B (FINITE DIFFERENCE METHOD)

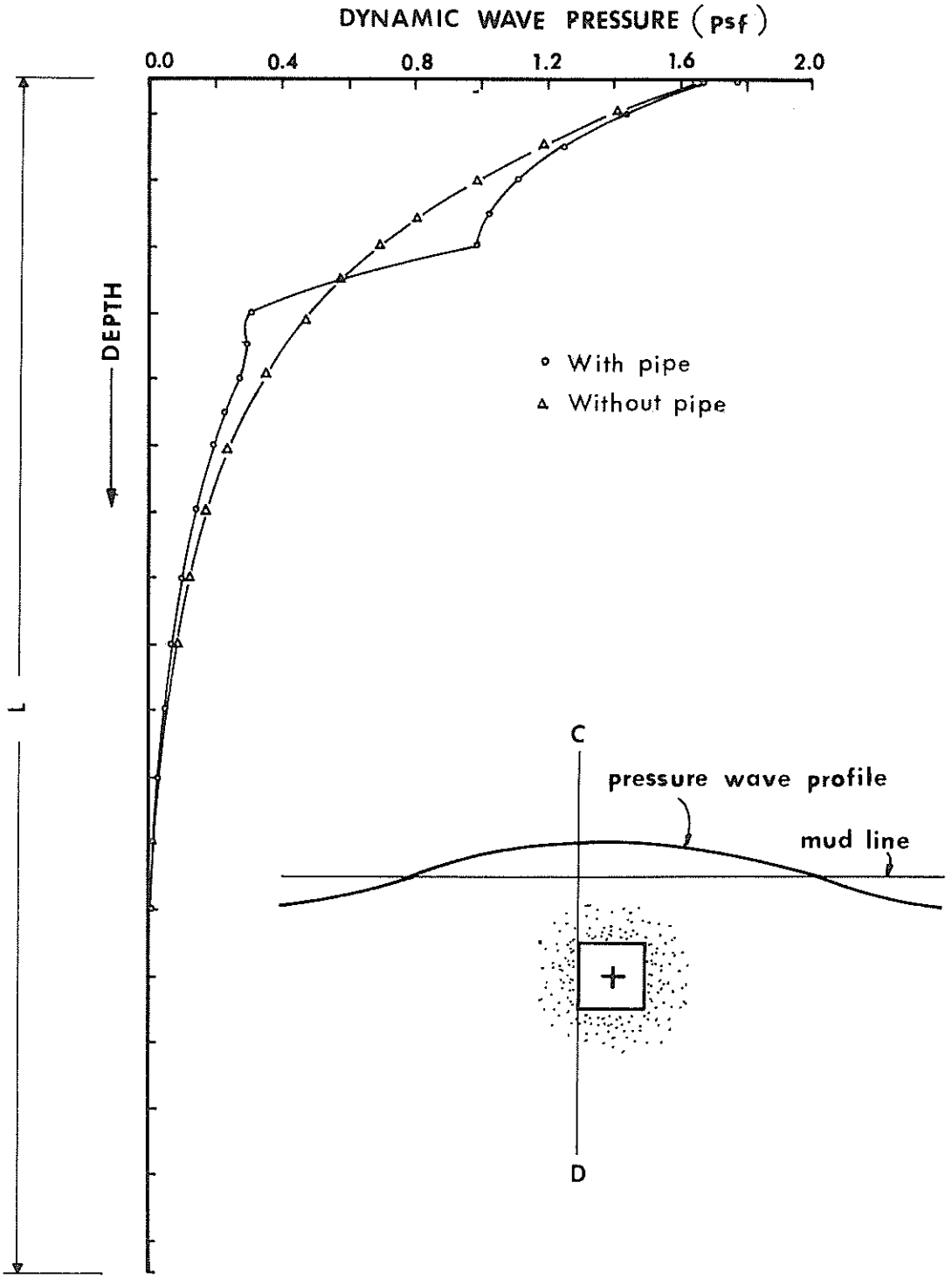

Fig. 6.12 - Effect of Pipe on Pressure in Soil along C—D
(Finite Difference Method)

plotted for the instants when t = T/4 (Fig. 6.13) and t = T/8 (Fig. 6.14). In this way, pressure variations at any point under a moving wave can be generated. The maximum pressure was found to occur at the instant when time t = 0, or when the pipe is directly under a wave crest or trough.

Finite Element Model

The finite element computer program (12) was applied to the same wave and soil conditions in Table 6.2 in a region as shown in Fig. 5.4. Fig. 6.15 shows a plot of the pressure values around a square pipe for the time instant of t = 0. A similar result was obtained as in the finite difference model, only that the increase in pressure at the top of the pipe is somewhat smaller in this case, and the decrease in pressure at the bottom is more pronounced. Figs. 6.16 - 6.18 show the finite element results for a circular pipe at different time instants under the same wave and soil conditions as above. Pressure values along the center line of the pipe are plotted in Fig. 6.19 for a wave profile as shown in the figure.

A comparison plot of the finite difference and finite element results are shown in Fig. 6.20. Due to an absence of experimental data in this study, a conclusive validation of the two methods was not possible. However, similar patterns of results were generally obtained by both methods in all cases. A definite conclusion can thus be drawn from these studies, that the introduction of an embedded pipe in a porous medium generally causes an increase of pressure at the

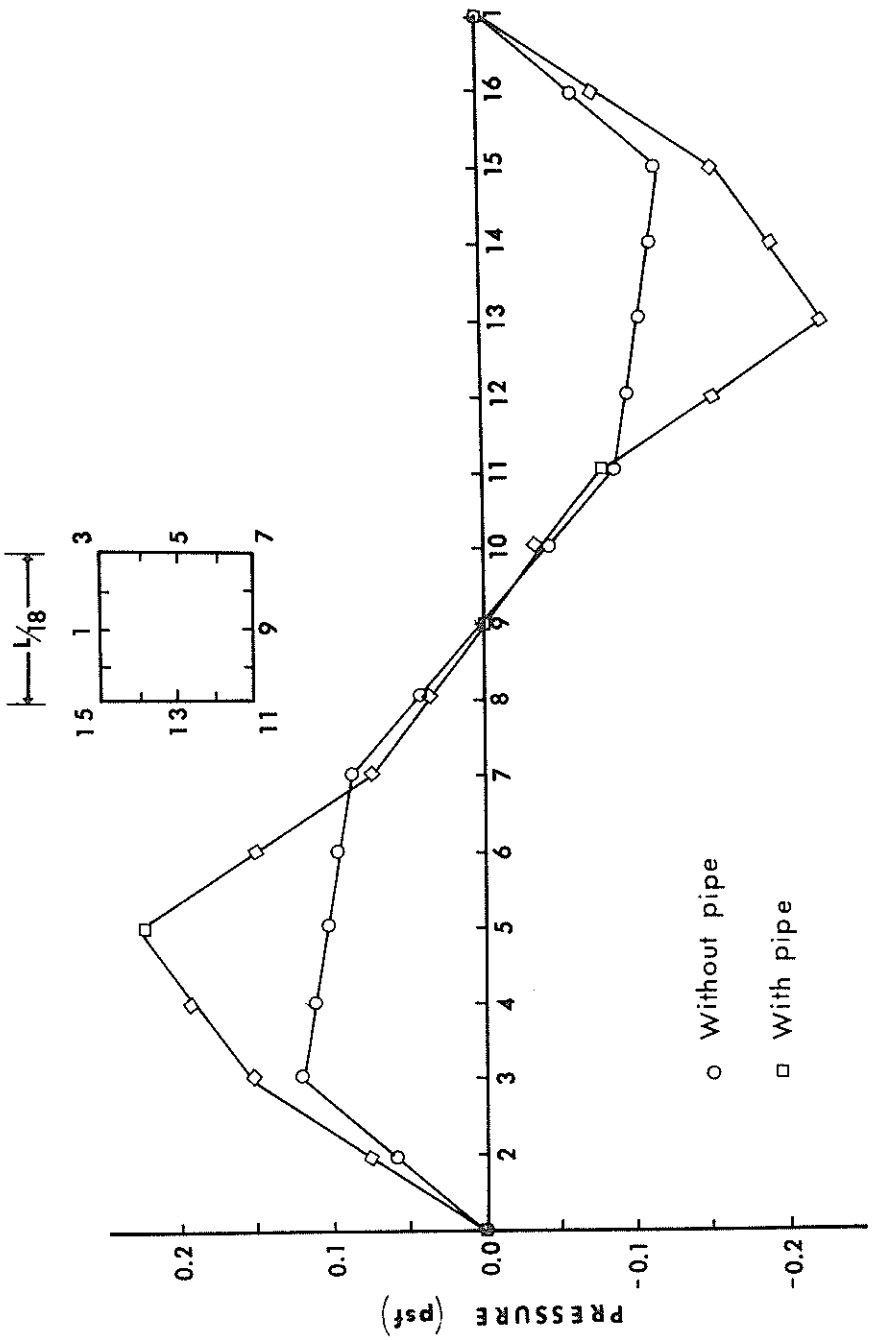

Fig. 6.13 - Pressure around a Square Pipe at t = T/4
(Finite Difference Method)

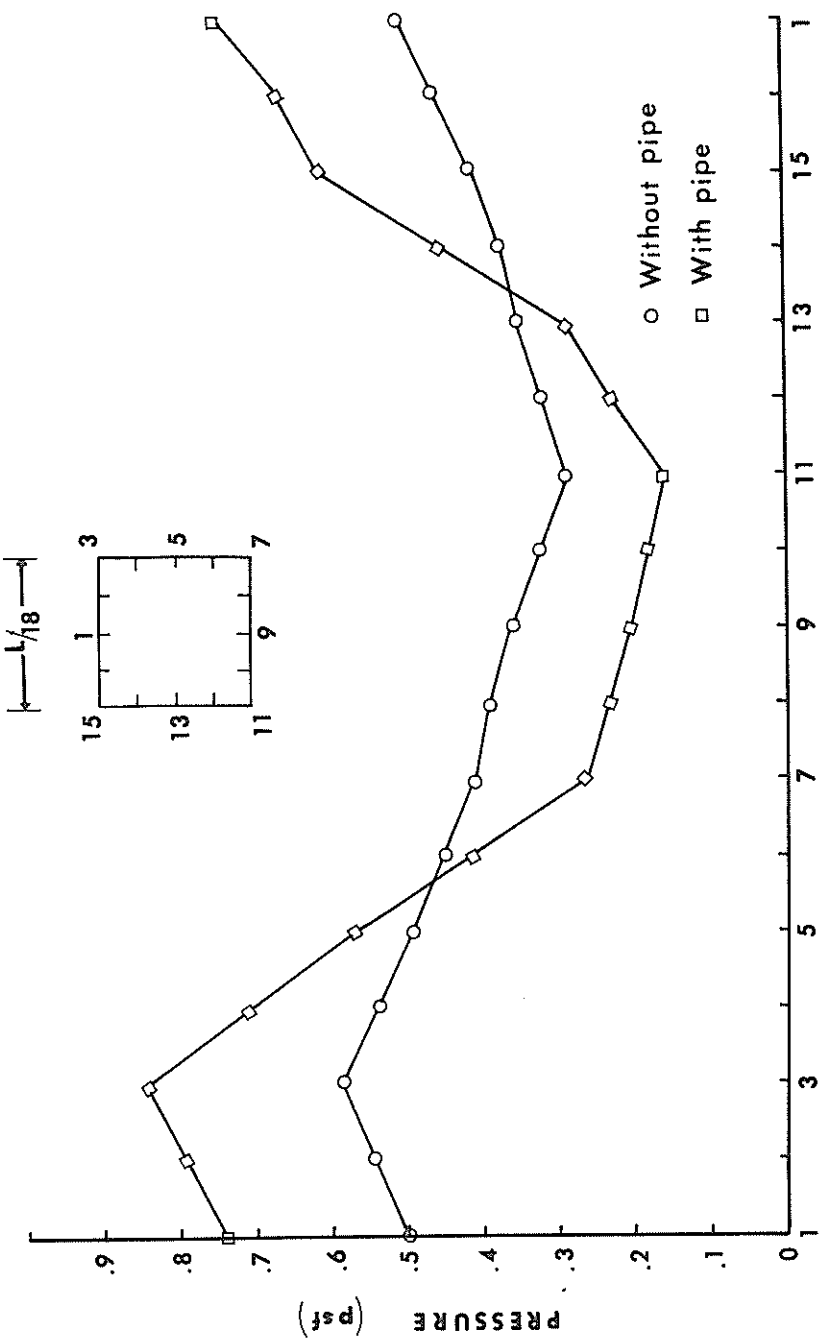

Fig. 6.14 - Pressure around a Square Pipe at t = T/8
(Finite Difference Method)

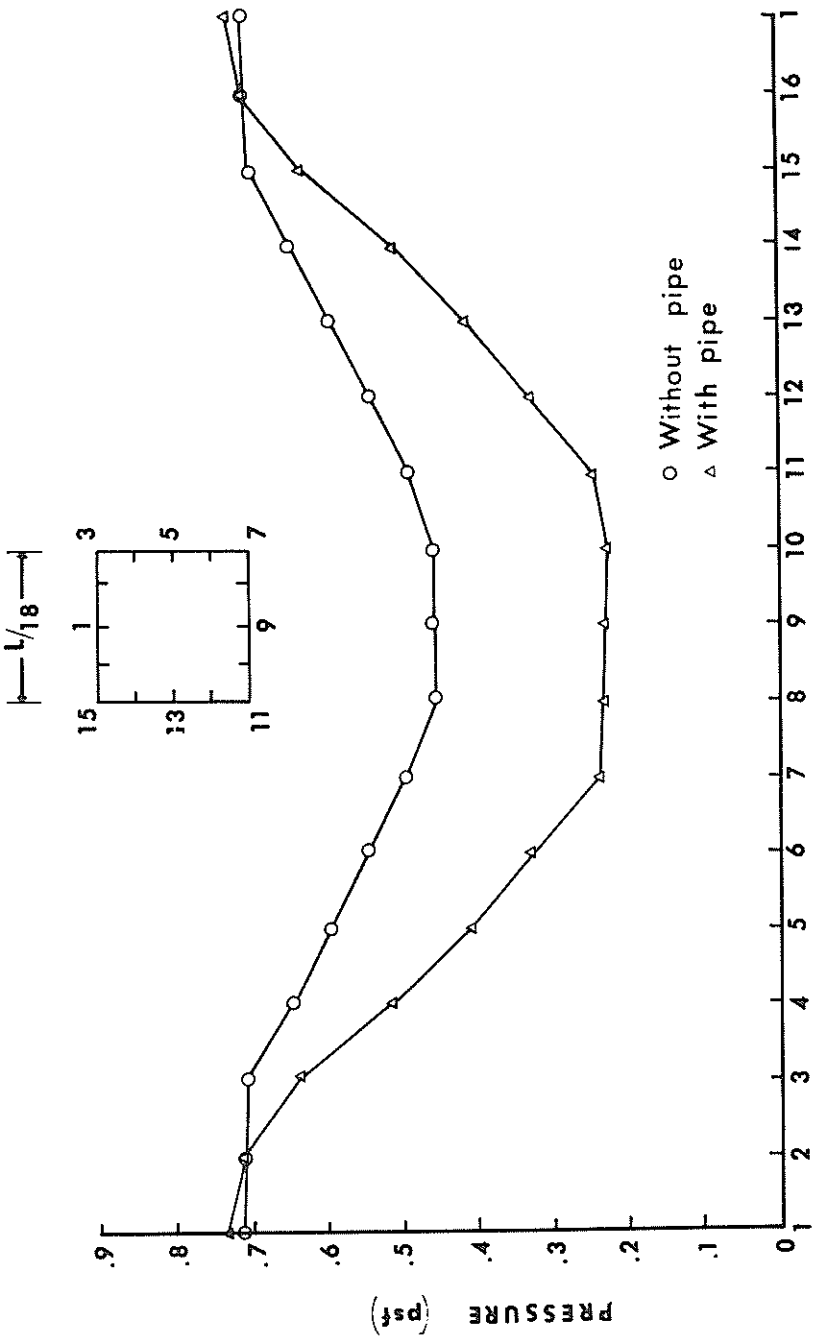

Fig. 6.15 - Pressure around a Square Pipe at t = 0
(Finite Element Method)

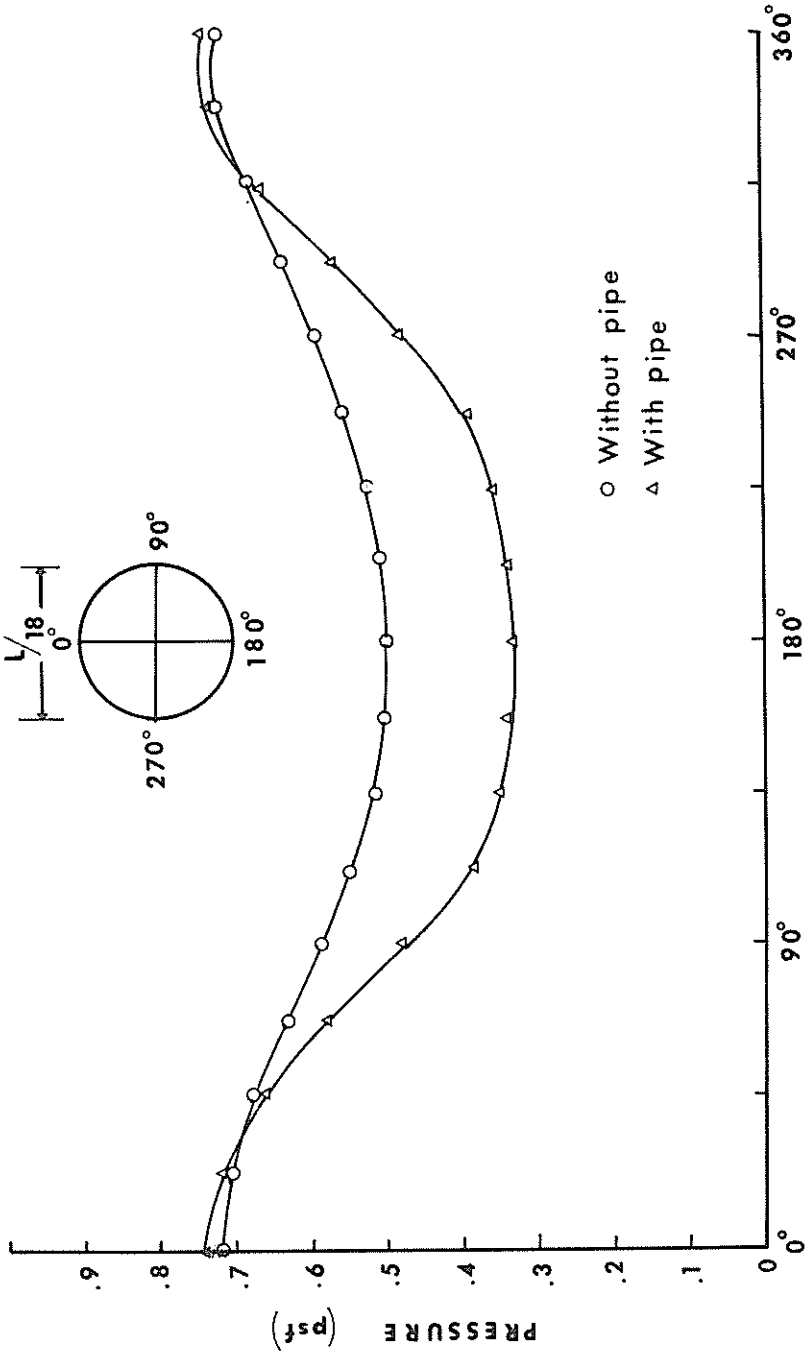

Fig. 6.16 - Pressure around a Circular Pipe at t = 0
(Finite Element Method)

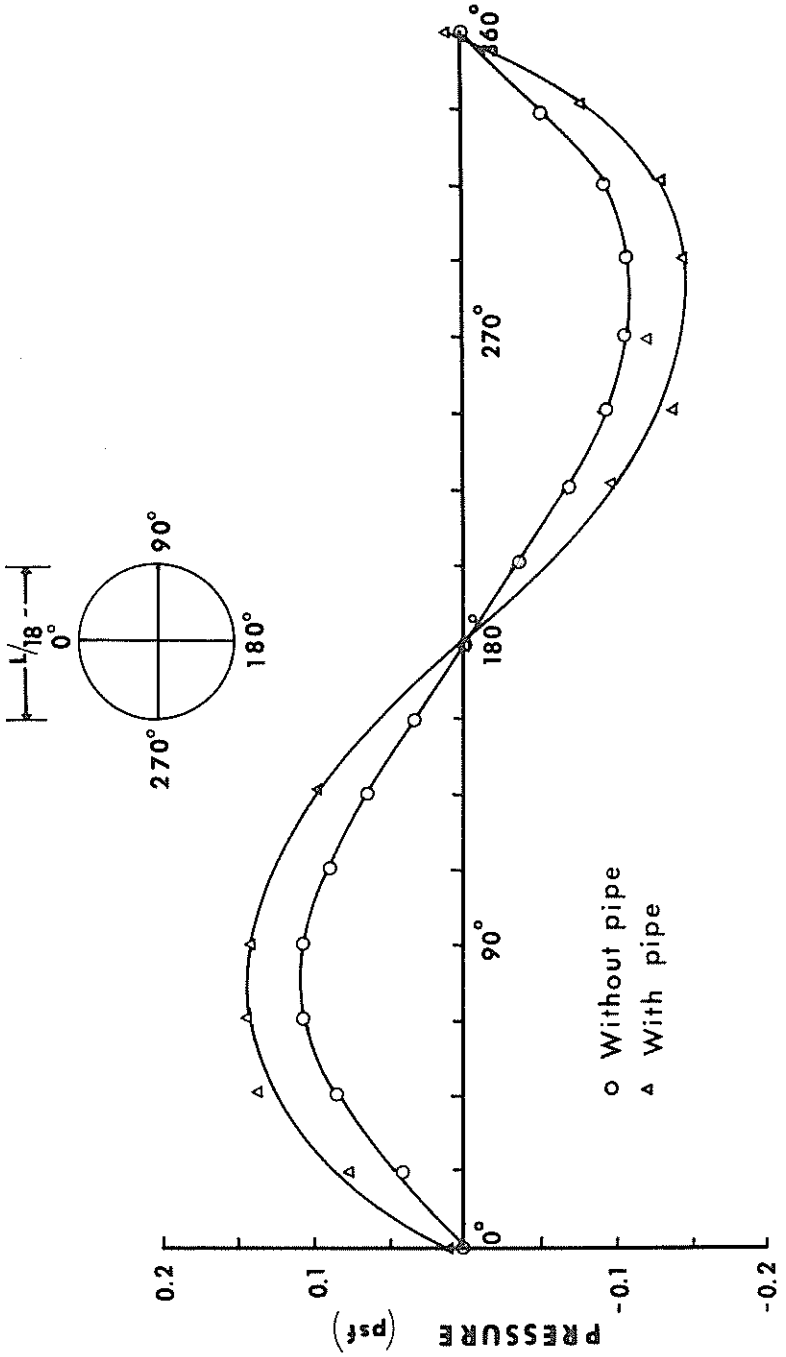

Fig. 6.17 - Pressure around Circular Pipe at t = T/4
(Finite Element Method)

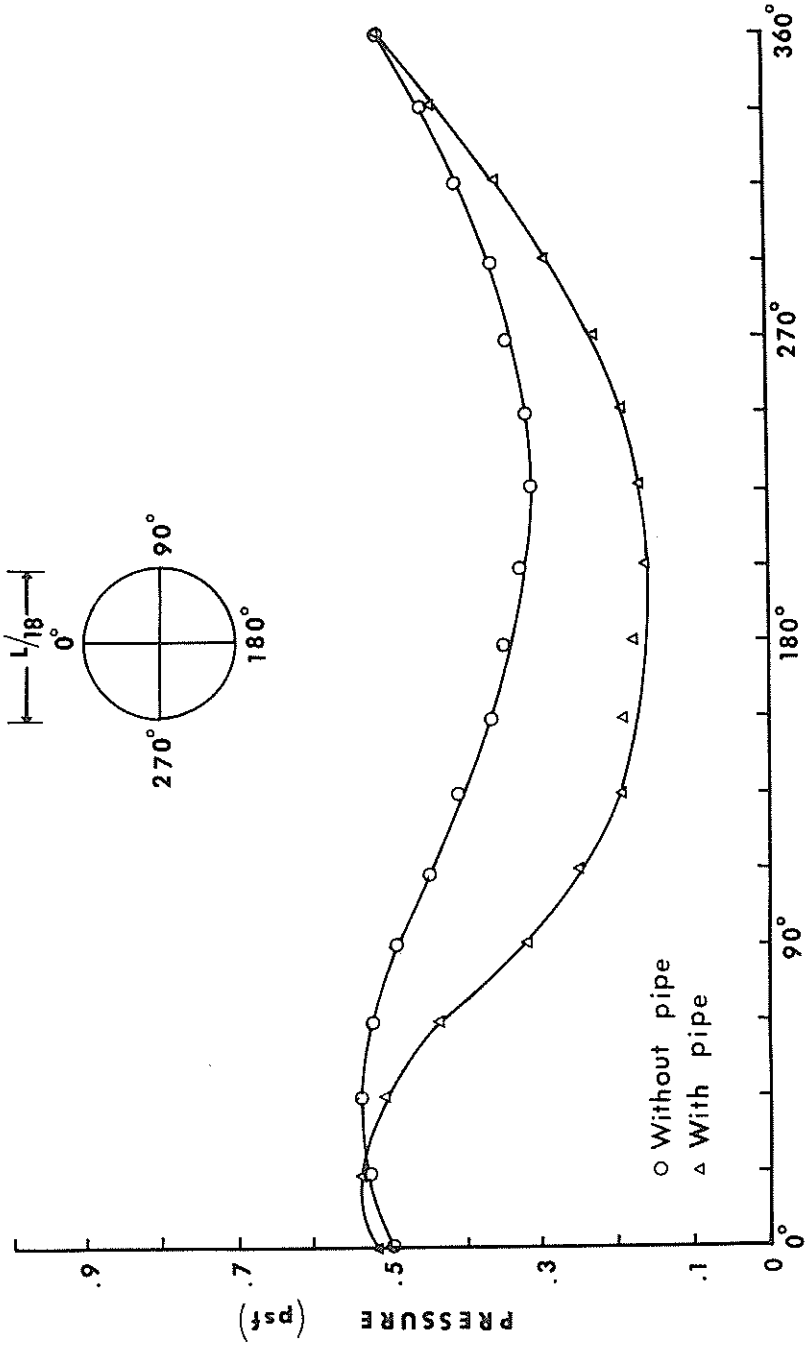

Fig. 6.18 - Pressure around a Circular Pipe at t = T/8
(Finite Element Method)

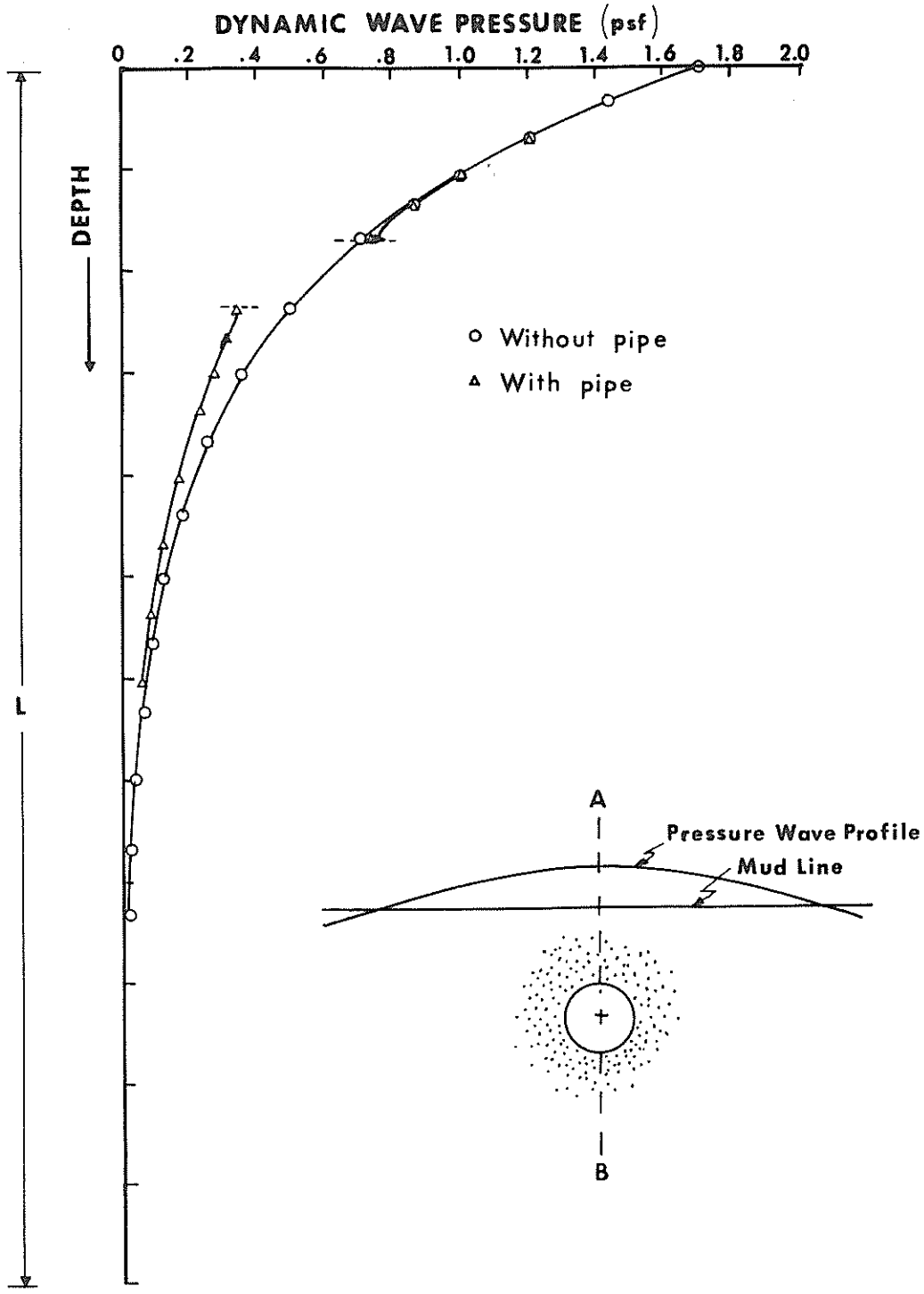

Fig. 6.19 - Effect of Pipe on Pressure in Soil along A-B
(Finite Element Method)

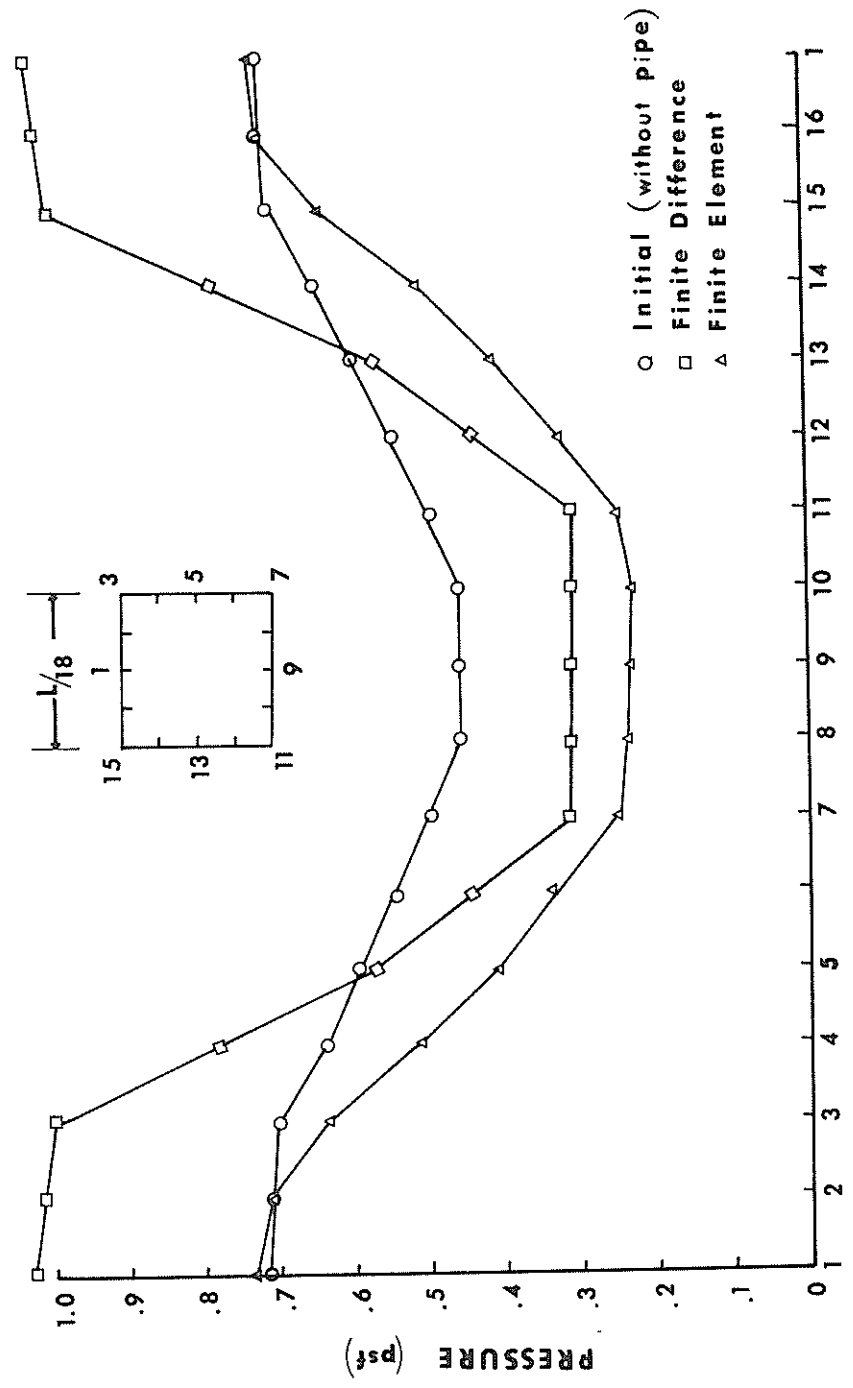

Fig. 6.20 - Pressure around a Square Pipe at t = 0
(Finite Element and Finite Difference)

top region of the pipe and a decrease at the bottom. The choice of a more reliable model between the finite difference and finite element methods lies on an assessment of accuracy of the two methods. In general, it can be shown that solutions obtained by the two methods for a certain regular mesh system are identical, and so are their orders of approximation (22). However, the presence of a specified gradient boundary condition on the pipe surface introduces differences between the two solutions. Better accuracy is expected in the finite element approach since the normal derivative condition on the pipe surface can be introduced naturally in the problem, while the finite difference approach depends on an approximation of the normal derivative equation, which again depends on mesh sizes which have to be comparable to the boundary layer thickness surrounding the embedded pipe. Nevertheless, the finite difference model is still useful to serve as a check on results obtained by the finite element approach.

Parameter Studies

In this section an effort will be made to illustrate the influence of several significant parameters on the pressure distribution around the pipe. The finite element scheme shown in Fig. 5.6 was used exclusively in this study.

Wave Height Variations

The influence of different wave heights on the distribution of pressure around a circular pipe was studied. A wave as shown in

item (1) of Table 6.1 provided the dynamic surface loading. Pressure values at the top and bottom of the pipe are plotted versus different wave heights in Figs. 6.21 and 6.22 respectively. Both figures show a linear relation in which pressure increases under increasing wave heights, and a greater gradient was observed in the second curve.

Wave Length Variations

A study was then made on the effect that different wave lengths have on the pressure distribution around the pipe. Wave height was kept at a constant 3.2 inches in all cases. The other parameters were the same as in the last section. Results are plotted in Fig. 6.23 in which pressure at a certain point on the pipe is shown to vary exponentially with changing wave lengths.

Pipe Size Variations

In this study, the center of the pipe was fixed at a depth of $\frac{3}{18}$ L and the diameter of the pipe was varied. A wave having a 3.2 inch height, a 1.62 second period and a length of 6.25 feet was used as a surface condition in each case. The resulting pressure at the top of the pipe in different pipe sizes is shown in Fig. 6.24. A nonlinear relation is evident in which pressure increases with increasing pipe sizes.

Burial Depth Variations

The effect of the depth of burial of a pipe was studied by

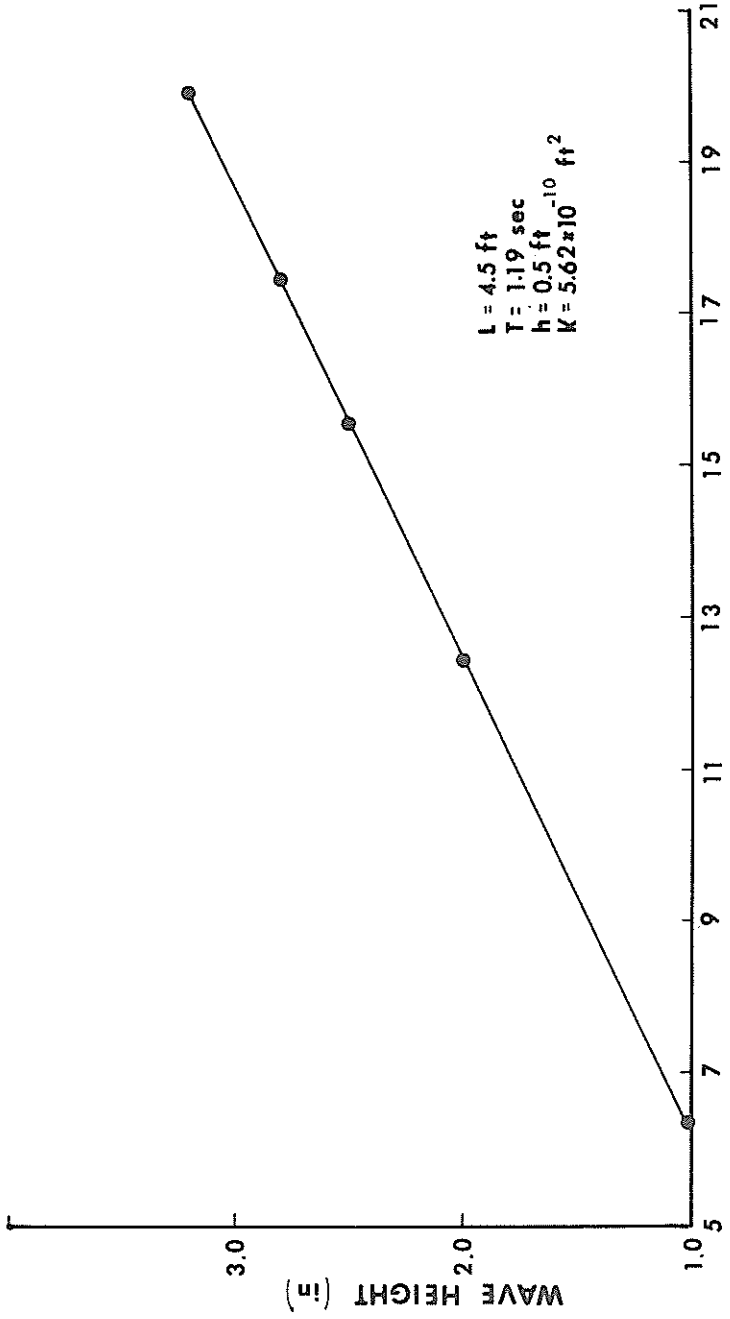

Fig. 6.21 - Effect of Wave Height on Pressure at Top of Pipe

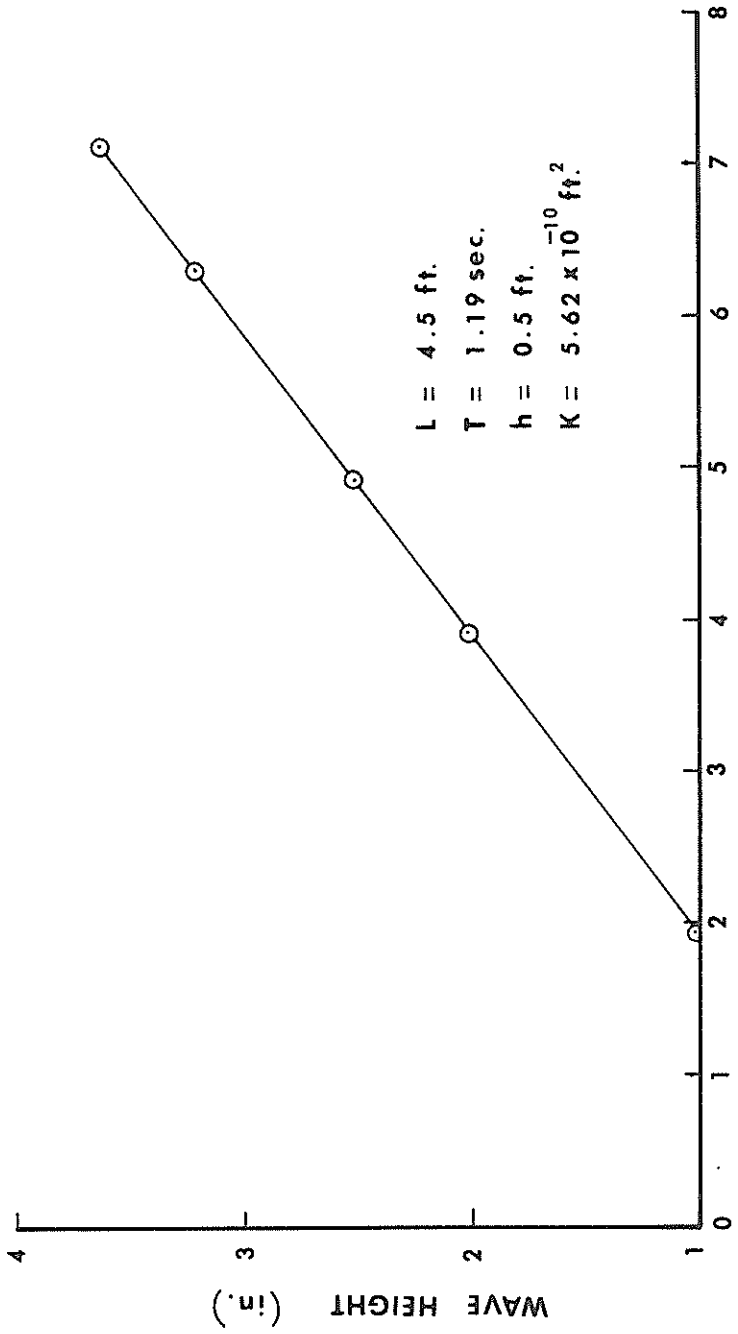

Fig. 6.22 - Effect of Wave Height on Pressure at Bottom of Pipe

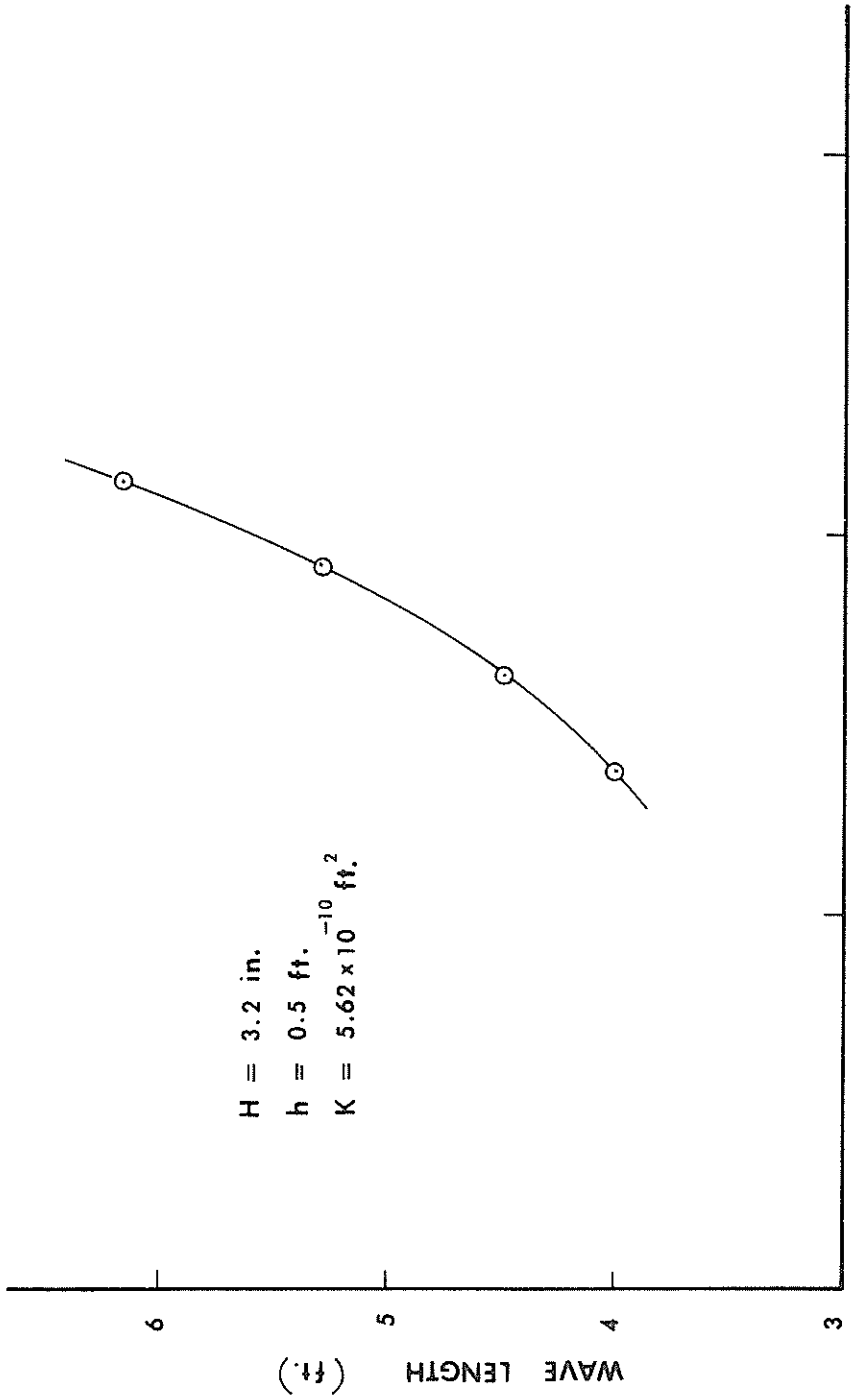

Fig. 6.23 - Effect of Wave Length on Pressure

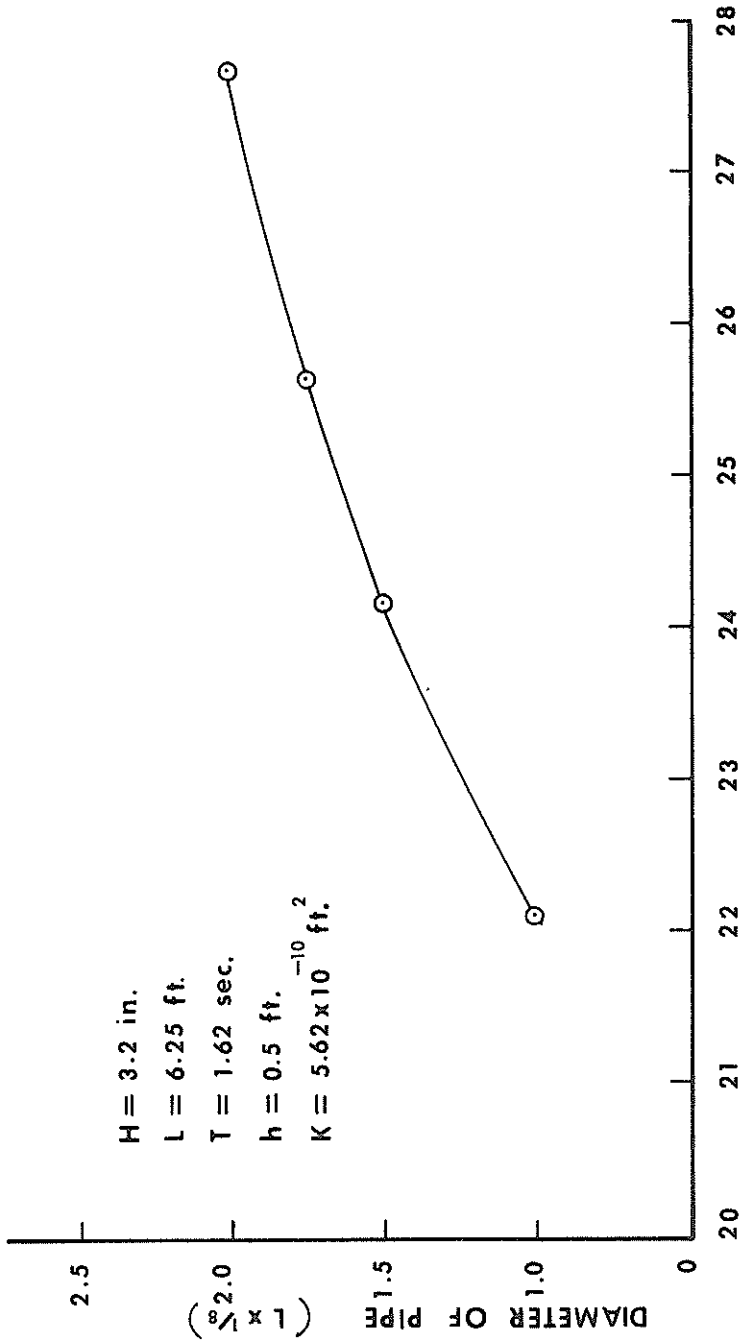

Fig. 6.24 - Effect of Pipe Size on Pressure at a certain Depth

moving the pipe down the center line of the region and solving the problem at different depths. The same wave conditions as in the last section were used in this study and the pipe diameter was set equal to L/18 in all cases. A resulting nonlinear curve is plotted in Fig. 6.25 showing a decrease of pressure with increasing burial depths.

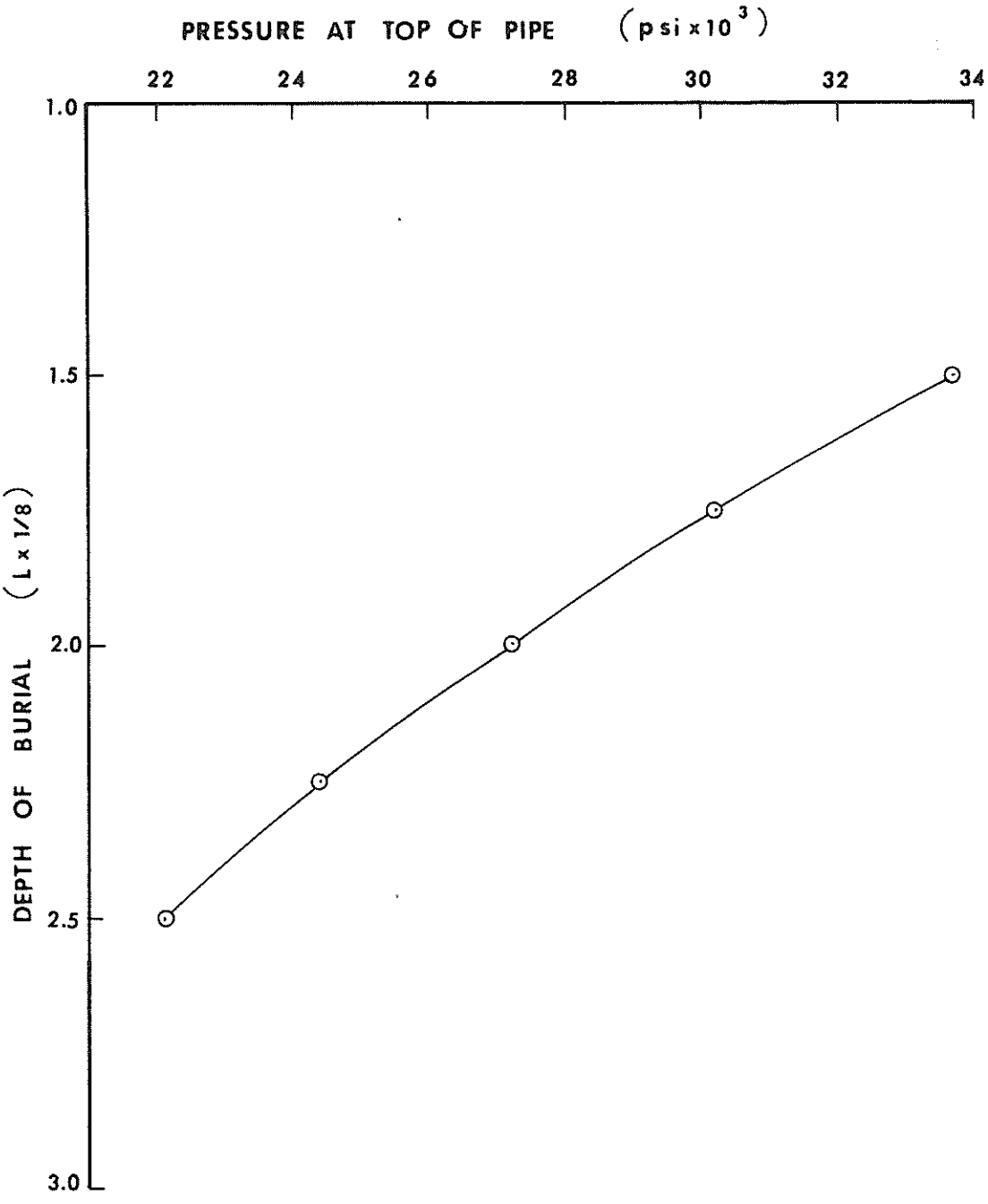

Fig. 6.25 - Effect of Depth of Burial on Pressure

CHAPTER VII

CONCLUSIONS AND REMARKS

The fundamental objective of this research was to develop a numerical model capable of determining the dynamic pressure distribution around a buried pipe under surface wave loading. Two approaches were proposed in this study, namely, the finite difference model and the finite element model. Both methods can be applied to study the influence of wave-pipe-soil interaction on the pressure distribution pattern by specifying different boundary conditions on the problem region.

A validation study of the two models applied to a flow region without an embedded pipe was undertaken by comparing the predicted results to those obtained from Liu's analytical solution and experimental data from a wave channel model study. The good comparisons obtained supported the extension and use of the models to evaluate the pressure distribution pattern around the embedded pipe in the flow region.

The general conclusions reached as a result of a limited parameter study are:

1. The introduction of a buried pipe into a region of porous medium influences the magnitude and distribution of the wave-induced dynamic pressure in the sediments surrounding the pipe.
2. The buried pipe causes an increase of pressure at the top region of the pipe and a decrease at the bottom.

3. The maximum pressure occurs when the crest or trough of the surface wave is directly over the pipe centerline.

4. The change of wave heights, wave lenghts, pipe sizes and burial depths of the pipe, all have definite influences on the pressure distribution pattern around the pipe.

The finite difference model produces slightly different results from the finite element model due to a complication of specified gradient boundary conditions on the pipe surface. The finite element model is expected to be more accurate and reliable as the gradient boundary condition is implemented naturally on the pipe surface. However, both numerical models can serve as a check on each other.

In summary, the development of the models described herein should serve to advance the "state-of-the-art" in analysis of buried offshore pipelines. The next logical step would be an incorporation of the proposed numerical models with more complete model tests in studying the buried pipeline stability problem.

CHAPTER VIII

RECOMMENDATIONS

The following areas are recommended for further research in extension of this study.

1. The numerical models developed were idealized to simulate a steady state situation for a perfectly drained condition in the porous medium. Wave-induced pressure is assumed to dissipate completely in the porous medium so that the build-up of pore water pressure by cyclic wave action as actually exists cannot at present be predicted by the models. The pore water pressure build-up phenomenon appears to be important in analyzing pipe flotation problems because it is thought that this build-up during storm conditions leads to liquefaction of bottom soil sediments. In order to better understand the entire dynamic situation, experimental tests should be performed to provide additional information so that corrective adjustments can be added to the numerical models.
2. The computer program might be modified to determine the effective stress values of soil sediments around the buried pipe so that results can be applied immediately in analysis of stability problems.
3. Higher order wave theories and heterogeneous soil conditions might be considered for incorporation with the numerical models.

APPENDIX I - REFERENCES

1. "ASCE Preliminary Research on Pipeline Flotation", Report of the Pipeline Flotation Research Council, Journal of the Pipeline Division, ASCE, Vol. 92, No. PL1, March 1966, pp. 27-65.

2. Bea, R.G., "How Sea Floor Slides affect Offshore Structures", The Oil and Gas Journal, Nov. 1971, pp. 88-92.

3. Blumberg, R., "Hurricane Winds, Waves and Currents test Marine Pipeline Design", Part 1 - Part 6, Pipeline Industry, June - November, 1964.

4. Brown, R.J., "How Deep Should an Offshore Line be Buried for Protection", The Oil and Gas Journal, Oct. 11, 1971, pp. 90-98.

5. Brown, R.J., "Rational Design of Submarine Pipelines", World Dredging and Marine Construction, Feb. 1971, pp. 17-22.

6. Brown, R.J., "Soil Mechanics Important in Marine Pipeline Construction", The Oil and Gas Journal, Sept. 16, 1957, pp. 151-155.

7. Campbell, S.J., "Interaction of Wave-Inducted Forces with Submarine Soils", unpublished master's thesis, Texas A&M University, 1974.

8. Christian, J.T., et al, "Large Diameter Underwater Pipeline for Nuclear Power Plant Designed Against Soil Liquefaction", Offshore Technology Conference, No. OTE 2094, May 1974, pp. 597-602.

9. Henkel, D.J., "The Role of Waves in Causing Submarine Landslides", Geotechnique, Vol. 20, No. 1, March 1970, pp. 25-70.

10. Hunt, J.N., "On the Damping of Gravity Wave Propagated Over a Permeable Surface", Journal of Geophysical Research, Vol. 64, 1959, pp. 437.

11. Ippen, A.T. (editor), Estuary and Coastline Hydrodynamics, McGraw-Hill Book Co., Inc., 1966.

12. Lai, N.W., "Computer Programs for Solving Pressure Distribution Around Buried Offshore Pipelines", unpublished report, Civil Engineering Dept., Texas A&M University, 1974.

13. Liu, P.L.F., "Damping of Water Waves over Porous Bed", Journal of the Hydraulics Division, ASCE, Vol.99, No. HY12, Paper 10218, Dec. 1973, pp. 2263-2271.

14. Murray, J.D., "Viscous Damping of Gravity Waves Over a Permeable Bed", Journal of Geophysical Research, Vol. 70, 1965, pp. 2325.

15. Putnam, J.A., "Loss of Wave Energy Due to Percolation in a Permeable Sea Bottom", Transaction of American Geophysical Union, Vol. 30, 1949, pp. 349.

16. Reid, R.O. and Kajiura, K., "On the Damping of Gravity Waves Over a Permeable Sea Bed", Transaction of American Geophysical Union, Vol. 38, 1957, pp. 662.

17. Savage, R.P., "Laboratory Study of Wave Energy Losses by Bottom Friction and Percoaltion", Technical Memo No. 31, Beach Erosion Board, 1953.

18. Seed, H.B. and Lee, K.L., "Liquefaction of Saturated Sands During Cyclic Loading", Journal of the Soil Mechanics and Foundations Division, ASCE, Vol. 92, No. SM6, Nov. 1966, pp. 105-134

19. Shaw, F.S., An Introduction to Relaxation Methods, Dover Publications, Inc., 1953.

20. Sleath, J.F.A., "Wave-Induced Pressure in Beds of Sand", Journal of the Hydraulics Division, ASCE, Vol. 96. No. HY2, Paper 7062, Feb. 1970, pp. 367-378.

21. Smith, G.D., Numerical Solutions of Partial Differential Equations, Oxford University Press, London, 1965.

22. Zienkiewicz, O.C., The Finite Element Method in Structural and Continuum Mechanics, McGraw-Hill Publishing Co., London, 1967.

APPENDIX II - NOTATION

The following symbols have been used in this report:

A	=	wave amplitude
B	=	depth of problem region
b	=	soil depth
D	=	pipe diameter
d	=	pipe burial depth
ESM	=	Element Stiffness Matrix
GSM	=	Global Stiffness Matrix
g	=	gravitational constant
H	=	wave height
h	=	still water depth
I	=	finite element functional
K	=	permeability
k	=	wave number
n	=	porosity
p	=	wave induced pressure
p_o	=	pressure at fluid-bed interface
p_1	=	pressure in upper fluid layer
p_2	=	pressure in porous bed
p'	=	hydrostatic pressure
p_b	=	boundary pressure value
$\bar{p}$	=	dimensionless pressure

SOR	=	Successive-Over-Relaxation
T	=	wave period
t	=	time
u	=	fluid particle velocity component in x-direction
v	=	fluid particle velocity component in y-direction
W	=	width of problem region
w	=	Successive-Over-Relaxation factor
$\overline{X}$	=	dimensionless distance in x-direction
x	=	horizontal coordinate
$\overline{Y}$	=	dimensionless distance in y-direction
y	=	vertical coordinate
ρ	=	mass density of water
ν	=	kinematic viscosity
σ	=	wave frequency